EUROPEAN ORGANIZATION FOR NUCLEAR RESEARCH

CERN-EP/85-54
19 April 1985

CALORIMETRY IN HIGH-ENERGY PHYSICS

C.W. Fabjan
CERN, Geneva, Switzerland

Lectures given at the
NATO Advanced Studies Institute on
Techniques and Concepts in High-Energy Physics (II)
St. Croix, Virgin Islands, USA, 2–13 August 1984

CALORIMETRY IN HIGH-ENERGY PHYSICS

Christian W. Fabjan

CERN

CH-1211 Geneva 23

1. INTRODUCTION

Much of our present knowledge about elementary particles has been established through a continuing refinement of techniques for measuring the trajectories of individual charged particles. Only in recent years has a different class of detectors—calorimeters—been widely employed, but these have already greatly influenced the scope of experiments.

Conceptually, a calorimeter is a block of matter which intercepts the primary particle, and is of sufficient thickness to cause it to interact and deposit all its energy inside the detector volume in the subsequent cascade or 'shower' of increasingly lower-energy particles. Eventually, most of the incident energy is dissipated and appears in the form of heat. Some (usually a very small) fraction of the deposited energy is detectable in the form of a more practical signal (e.g. scintillation light, Cherenkov light, or ionization charge), which is proportional to the initial energy.

The first large-scale detectors of this type were used in cosmic-ray studies [1]. Interest in calorimeters grew during the late 1960's and early 1970's in view of the new accelerators at CERN [the Intersecting Storage Rings (ISR) and the Super Proton Synchrotron (SPS)] and at the Fermi National Accelerator Laboratory (FNAL), with their greatly changed experimental directions and requirements [2]. One consequence of the new fixed-target accelerators was the advent of intense, high-energy neutrino beams with the need for very massive detectors to study their interactions. This detector development was paralleled by the rapid growth of analog signal-processing techniques: during the last decade the typical number of analog signal-channels of nuclear spectroscopy quality has increased from about 10 to 10^4 in high-energy physics experiments.

Calorimeters offer many attractive capabilities, supplementing or replacing information obtained with magnetic spectrometers:

1) They are sensitive to charged and neutral particles.
2) The 'energy degradation' through the development of the particle cascade is a statistical process, and the average number $\langle N \rangle$ of secondary particles is proportional to the energy of the incident particle. In principle, the uncertainty in the energy measurement is governed by statistical fluctuations of N, and hence the relative energy resolution σ/E improves as $1/\sqrt{\langle N \rangle} \sim E^{-1/2}$.
3) The length of the detector scales logarithmically with particle energy E, whereas for magnetic spectrometers the size scales with momentum p as $p^{1/2}$, for a given relative momentum resolution $\Delta p/p$.
4) With segmented detectors, information on the shower development allows precise measurements of the position and angle of the incident particle.
5) Their different response to electrons, muons, and hadrons can be exploited for particle identification.
6) Their fast time response allows operation at high particle rates, and the pattern of energy deposition can be used for rapid on-line event selection.

In these notes we comment first on the principal features of detectors designed to measure the energy of photons and electrons, the 'electromagnetic shower detectors' (ESD). The underlying physics has been understood for many years, and such detectors were the main components in many experiments—some of which were credited with important discoveries. Recent developments have been emphasizing precision measurements of energy and position in large arrays.

In the subsequent section the physics of 'hadronic calorimeters' is reviewed. Progress during the last decade contributed to an understanding of the physics of this technique and to a steadily growing range of applications.

The final section concentrates on the technical issues of information processing from calorimeters. We can only select representative examples from the numerous and ingenious methods devised to extract the energy information. We end with a discussion on the state-of-the-art Monte Carlo simulation of electromagnetic and hadronic showers.

These notes follow an earlier review [3], emphasize recent developments, update the bibliography, but do not supersede other excellent introductions to this field [4, 5].

2. ELECTROMAGNETIC SHOWER DETECTORS

2.1 Energy Loss Mechanism

The contributions of the various energy loss mechanisms as a function of particle energy are given in Fig. 1 for electrons and positrons and in Fig. 2 for photons [6]. Above approximately 1 GeV, the principal processes—bremsstrahlung for electrons and positrons, pair production for photons—become energy independent. It is through a succession of these energy loss mechanisms that the electromagnetic cascade (EMC) is propagated, until the energy of the charged secondaries has been degraded to the regime dominated by ionization loss. Within this description, the combined energy loss of the cascade particles in the detector equals the energy of the incident electron or photon. The measurable signal—excitation or ionization of the medium—can be considered as the sum of the signals from the track segments of the positrons and electrons. Naively one might therefore expect that this signal should be equivalent to that produced by muons traversing the detector and whose combined track length equals that of the track

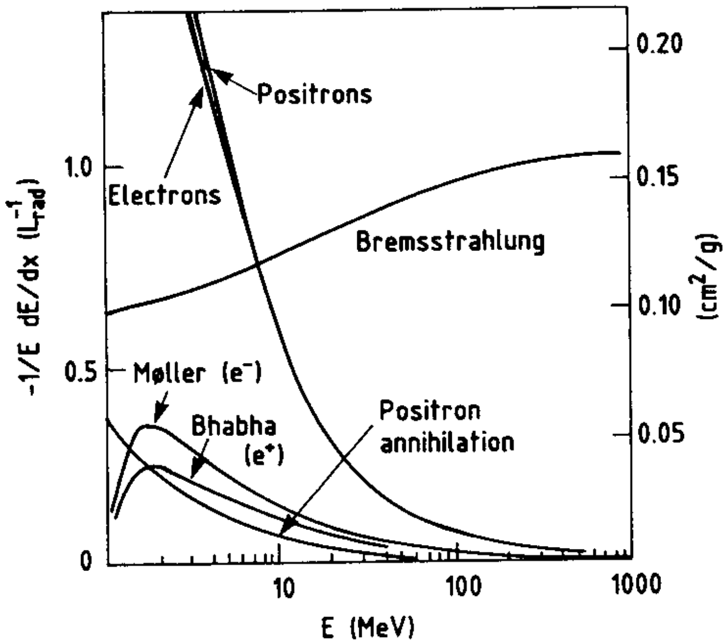

Fig. 1: Fractional energy loss per radiation length (left ordinate) and per g/cm^2 (right ordinate) in lead as a function of electron or positron energy. (Review of Particle Properties, April 1982 edition).

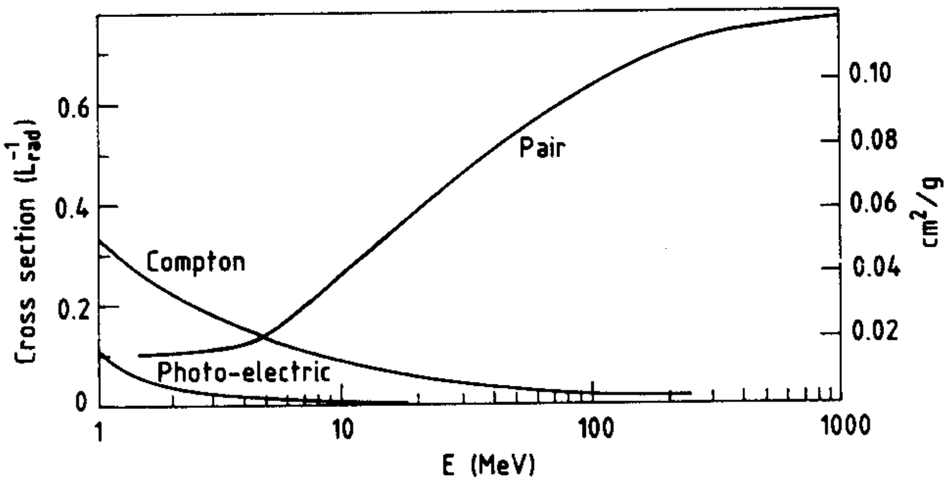

Fig. 2: Photon cross-section σ in lead as a function of photon energy. The intensity of photons can be expressed as $I = I_0 \exp(-\sigma x)$, where x is the path length in radiation lengths. (Review of Particle Properties, April 1980 edition).

segments of the EMC. This picture ignores finer points concerning low-probability photo-nuclear interactions, non-linear response of the ionizing medium as a function of ionization density or the detailed response to the very low energy e^+'s or e^-'s of the last generation of the shower. It emphasizes, however, the concept of 'track length T': a calorimeter is a useful device, because in the process of cascade formation the total track length T required for absorption is broken up into a 'tree' of many individual segments.

The electromagnetic cascading is fully described by quantum electrodynamics (QED) [7], and depends essentially on the density of electrons in the absorber medium. For this reason it is possible to describe the characteristic longitudinal dimensions of the high-energy EMC ($E > 1$ GeV) in a material-independent way, expressed by the 'radiation length, X_0'. It is defined through the equation for the energy loss $\Delta E/\Delta x$ *by radiation*

$$(\Delta E/\Delta x)_{\mathrm{radiation}}\,[X_0^{-1}] = -E$$

and the numerical value is well approximated by the following expression:

$$X_0\,[\mathrm{g/cm^2}] \simeq 180\,A/Z^2 \text{ (to better than 20\% for } \simeq Z > 13).$$

Whilst the high-energy part of the EMC is governed by the value of X_0, the low-energy tail of the shower is characterized by the 'critical energy ϵ' of the medium. It is defined as the energy loss *by collisions* of electrons or positrons of energy ϵ in the medium per unit X_0, i.e.

$$(dE/dx)_{\mathrm{collision}}\,[X_0^{-1}] = -\epsilon, \qquad \text{where } \epsilon\,(\mathrm{MeV}) \simeq 550 \times Z^{-1}$$

(accurate to better than 10% for $Z > 13$). This value of ϵ coincides approximately with that value of the electron energy below which the ionization energy loss starts to dominate the energy loss by bremsstrahlung. The critical energy ϵ is seen to define the dividing line between shower multiplication and the subsequent dissipation of the shower energy through excitation and ionization.

A rigorous, analytical description of the longitudinal shower profile has been given by Rossi [8] based on the following assumptions ('Rossi's approximation B'), and the most useful results are given in Table 1:

i) the cross-section for ionization is energy independent, $dE/dx\,[X_0^{-1}] = -\epsilon$;
ii) multiple scattering is neglected and the EMC is treated one-dimensionally;
iii) Compton scattering is neglected.

Table 1: EMC Quantities Evaluated with Rossi's Approximation B
($y = E/\epsilon$; T measured in units of X_0)

	Incident electron	Incident photons
Peak of shower, t_{max}	$1.0 \times (\ln y - 1)$	$1.0 \times (\ln y - 0.5)$
Centre of gravity, t_{med}	$t_{max} + 1.4$	$t_{max} + 1.7$
Number e^+ and e^- at peak	$0.3\,y \times (\ln y - 0.37)^{-1/2}$	$0.3\,y \times (\ln y - 0.31)^{-1/2}$
Total track length T	y	y

The characteristic longitudinal EMC profile is shown in Fig. 3 for four very different materials and demonstrates the 'longitudinal scaling in radiation length'. A convenient analytical description of the profile has been given in the form [9]

$$dE/dt = E_0\,b^{\alpha+1}/\Gamma(\alpha+1)\,t^{\alpha}e^{-bt}\,;\; t = x/X_0\,,\; \alpha = bt_{max}, \text{ and } b \simeq 0.5\,.$$

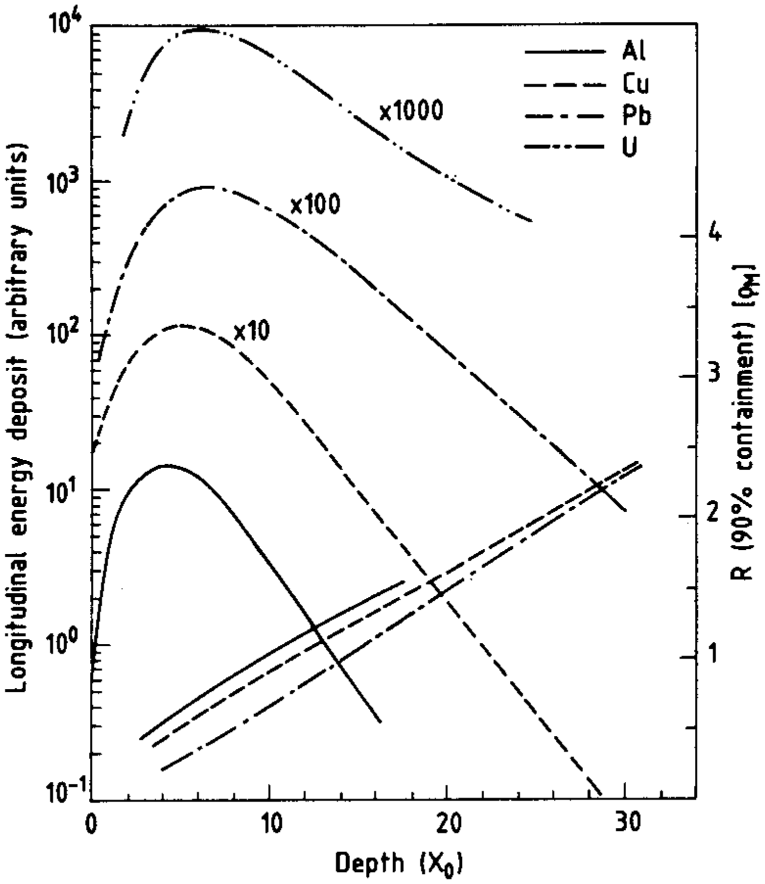

Fig. 3: Longitudinal shower development (left ordinate) of 6 GeV/c electrons in four very different materials, showing the scaling in units of radiation lengths X_0. On the right ordinate the shower radius for 90% containment of the shower is given as a function of the shower depth. In the later development of the cascade, the radial shower dimensions scale with the Molière radius $\varrho_M \sim 7A/Z$. [Al, Cu, and Pb, adapted from G. Bathow et al., Nucl. Phys. B20:592 (1970). Uranium data from G. Barbiellini et al., Ref. [127].

The transverse shower properties, which are not described within the framework of Rossi's 'approximation B' can also be easily understood qualitatively. In the early, most energetic part of the cascade the lateral spread is characterized by both the typical angle for bremsstrahlung emission, $\theta_{\mathrm{brems}} \sim p_e/m_e$, and multiple scattering in the absorber. This latter process increasingly influences the lateral spread with decreasing energy of the shower particles and causes a gradual widening of the shower. For the purpose of total energy measurement, the EMC occupies a cylinder of radius R

$$R \approx 2\varrho_M \, ; \qquad \varrho_M = 21X_0/\epsilon \simeq 7A/Z \; [\mathrm{g\,cm^{-2}}],$$

ϱ_M being the 'Molière Radius', which describes the average lateral deflection of electrons of energy ϵ after traversing one radiation length. In Fig. 4, the transverse shower profile as a function of depth clearly exhibits the rather pronounced central and energetic core surrounded by a low-energy 'halo'.

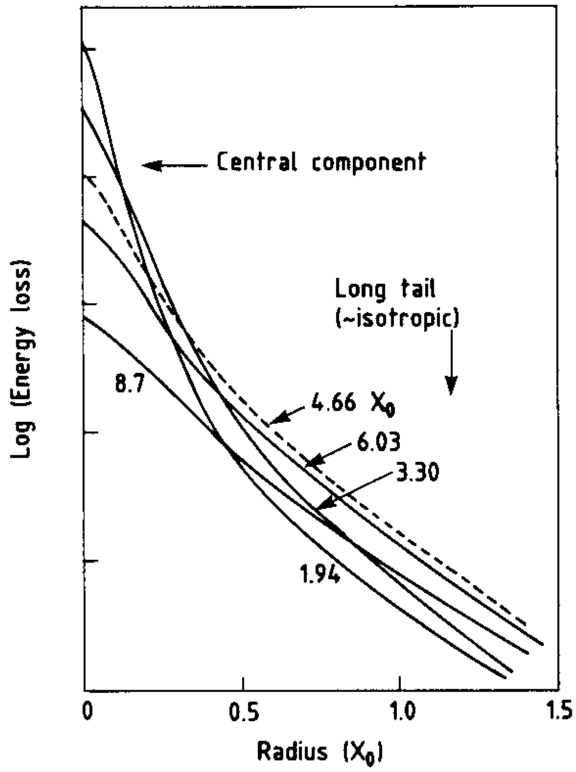

Fig. 4: Radial shower profile of 1 GeV electrons in aluminium; a pronounced central core, surrounded by 'halo', gradually widens with increasing depths of the shower [17].

2.2 Limits on Energy Resolution of EMCs

In the discussion in the previous section we have represented the shower by a total track length T, which could be expressed as $T(X_0) = E_{particle}(MeV)/\epsilon(MeV)$. The 'detectable' track length T_d, i.e. the equivalent track length which corresponds to the measured signal in a particular detector, will in general be shorter, $T_d \leq T$, as practical devices are only sensitive to the cascade particles above a certain threshold energy η. The fractional reduction in visible track length as a function of η/ϵ [4] is indicated in Fig. 5. The dotted lines are the result of an analytic calculation [8] for $E \gg \eta$, and $F(\xi)$ is given by $F(\xi) = [1+\xi \ln(\xi/1.53)] \exp \xi$ ($\xi = 2.29\ \eta/\epsilon$). The points are obtained by Monte Carlo calculations [9–11].

The average detectable track length $\langle T_d \rangle$ is given by $\langle T_d \rangle (X_0) = F(\xi) \cdot E/\epsilon$ and calorimetric energy measurements are possible because $\langle T_d \rangle \propto E$ for any reasonable value of ϵ. The *resolution* of the energy measurement is determined by the *fluctuations* in the shower propagation. The intrinsic component of the resolution is caused by the fluctuations in T_d. This represents the lower bound on the energy resolution and may be qualitatively estimated in the following way: the maximum number of track segments $N_{max} = E/\eta$ hence $\sigma(E)/E \geq \sigma(N_{max})/N_{max}$. In a lead-glass shower counter for which $\eta \sim 0.7$ MeV, one estimates for a 1 GeV shower, $N_{max} = 1000/0.7 = 1.5 \times 10^3$, implying an energy resolution at the level of one to two percent, somewhat higher than the level computed by detailed Monte Carlo calculations [9].

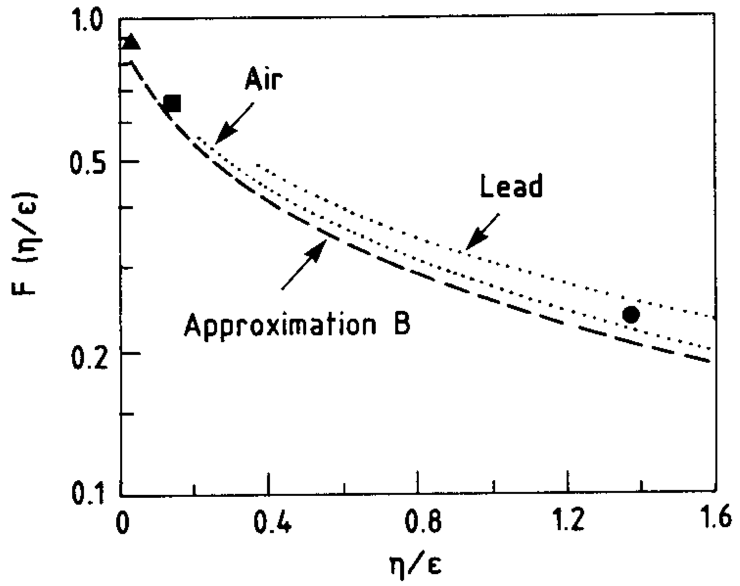

Fig. 5: Fraction F of the total track length which is seen on the average in a fully contained electromagnetic shower. The dotted lines represent analytical calculations and the points represent Monte Carlo results. ▲: lead glass; ■ and ●: lead sampling devices (see Ref. [4]).

In practical detectors, however, usually a number of additional components must be considered, which may conspire to affect the resolution. One important instrumental contribution to the energy resolution comes from incomplete containment of the showers ('energy leakage'), as can be seen from Fig. 6. Available information on average longitudinal containment (both experimental and calculational) may be parametrized as

$$L(98\%)_{av} \simeq t_{max} + 4\,\lambda_{att},$$

where L(98%) gives the length for 98% longitudinal containment. The quantity λ_{att} characterizes the slow, exponential decay of the shower after the shower maximum (see Fig. 3) expressed as $\exp(-t/\lambda_{att})$. The values of λ_{att} are found to be rather energy independent, but material dependent and close in value to the mean free path of photons that have minimum attenuation in a given material. Experimental values cluster around $\lambda_{att}\,[X_0] \simeq 3.4 \pm 0.5 X_0$. This estimate is in reasonable agreement with other parametrizations [12], e.g. $L(98\%) \simeq 2.5\,t_{max}$ for E in the 10 to 1000 GeV range. The effect of longitudinal leakage on the energy resolution is consistent with the parametrization

$$\sigma(E)/E \simeq [\sigma(E)/E]_{f=0} \times [1 + 2\sqrt{E(\mathrm{GeV})} \times f]$$

for values f of the fractional energy loss through leakage, $f < 0.2$ and $E < 100$ GeV. One notes that longitudinal leakage is more critical than transverse leakage due to the fact that fluctuations about the average longitudinal loss are much larger than for transverse leakage.

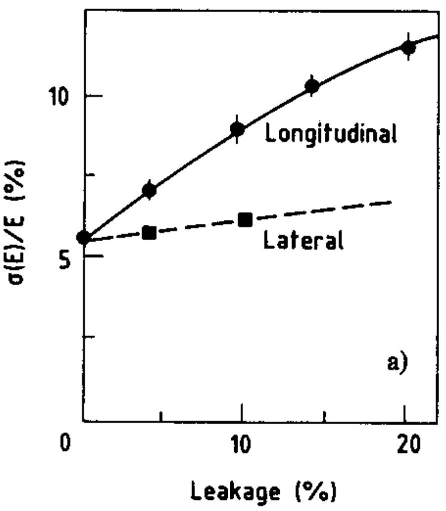

Fig. 6a: Effects of longitudinal and lateral losses on the energy resolution as measured for electrons in the CHARM neutrino calorimeter [23].

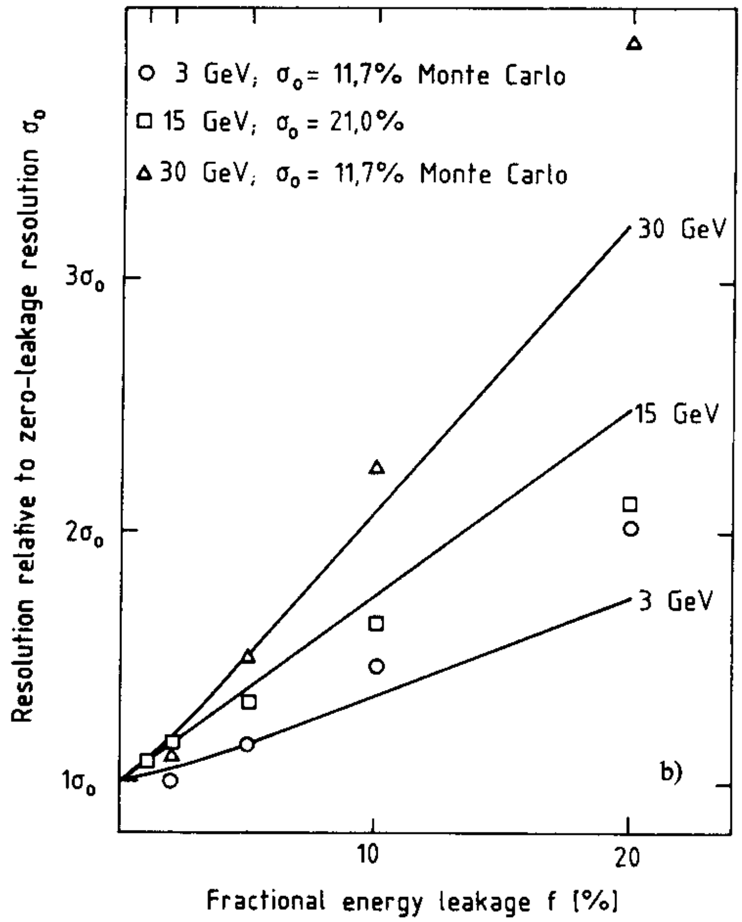

Fig. 6b: Deterioration of the zero-leakage resolution σ_0 as a function of fractional energy leakage f for three different electron energies [21, 23].

Homogeneous detectors have always played a very important role as e.m. calorimeters. Historically, it was NaI that was used as one of the first calorimetric detectors, still unsurpassed in energy resolution. For energies E = 1 GeV, one obtains a value close to the intrinsic limit; at higher energies, the full statistical gain ~ $1/\sqrt{E}$ is not obtained, even for very carefully tuned instruments [13] for which the resolution is quoted as $\sigma(E)/E \simeq 0.009 \times E^{-1/4}$ (GeV). Such a behaviour is characteristic of contributions other than those governed by statistical processes, such as non-uniformity in the signal collection, energy leakage, etc. A second, very frequently used homogeneous detector is lead glass, i.e. glass loaded with 50–60% PbO. The EMC is sampled by the production of Cherenkov light emitted from the relativistic electron-positron pairs. These detectors are therefore characterized by a relatively low light yield—typically 1000 photoelectrons per GeV are measured—and a relatively large cut-off energy η. These two effects combined give a resolution of

$$\sigma_{\text{tot}} = (\sigma_\eta^2 + \sigma_{\text{ph}}^2)^{1/2} \simeq (0.020^2 + 0.032^2)^{1/2} = 3.8\% \text{ at } 1 \text{ GeV},$$

in agreement with the best values reported, of $\gtrsim$ 4%. Recent developments of new scintillating crystals have stimulated interest in such homogeneous detectors, which promise exceedingly good performance in the 1 to 100 GeV regime (see the discussion in Section 5).

2.3 Energy Resolution in 'Sampling' Calorimeters

'Sampling' calorimeters are devices in which the functions of energy degradation and energy measurement are separated in alternating layers of different substances. This allows a considerably greater freedom in the optimization of detectors for certain specific applications. The choice of a 'passive' absorber—typically plates made of Fe, Cu, or Pb, each ranging in thickness from a fraction of X_0 to a few X_0—makes it possible to build rather compact devices, and it permits optimization for a specific experimental requirement such as electron/pion discrimination or position measurement. Independently of the choice of the absorber, the readout method may be selected for best uniformity of signal collection, high spatial subdivision, rate capability or other criteria. The disadvantage is that only a fraction of the total energy of the EMC is 'sampled' in the active planes, resulting in additional *'sampling' fluctuations* of the energy determination.

These general comments apply to both electromagnetic and hadron calorimeters. The following discussion of sampling fluctuations is specifically valid for the measurement with e.m. calorimeters, for which sampling fluctuations have been rather carefully studied. Today we know that they depend on the characteristics of both the passive and the active medium (in particular, thickness and density) and that several effects contribute to the 'total' sampling fluctuation.

The *'intrinsic sampling' fluctuations* express the statistical fluctuations in the number of e^+e^- pairs traversing the active signal planes and can be estimated in the spirit of approximation B. The number N_x of crossings is (η = 0)

$$N_x = T \text{ (total track length)}/d \text{ (distance between active plates)},$$

where $T = E/\epsilon$ and hence $N_x = E/\epsilon d = E/\Delta E$, ΔE being the energy loss per unit cell.

The contribution to the energy resolution is

$$\sigma(E)/E_{sampling} = \sigma(N_x)/N_x = 1/\sqrt{N_x} = 3.2\% \, [\Delta E\,(\mathrm{MeV})/E\,(\mathrm{GeV})]^{1/2}.$$

This expression has to be regarded as a lower bound on the sampling fluctuations for the following reasons:

- tracks originate from pair-produced particles and therefore the number of independent gap crossings would be only $N_x/2$ for totally correlated production;

- approximation B ignores multiple scattering, which increases the effective distance d to $d = d/\langle\cos\theta\rangle$, where the characteristic multiple scattering angle θ is given by $\langle\cos\theta\rangle \sim \cos(21\ \mathrm{MeV}/\epsilon\pi)$ [4];

- for $\eta \neq 0$, $T_d = F(\xi)T$.

Considering these effects, the contribution of sampling fluctuations to the energy resolution is evaluated as

$$[\sigma(E)/E]_{sampling} \gtrsim 3.2\% \, \{\Delta E\,(\mathrm{MeV})/[F(\xi) \times \cos(21/\epsilon\pi)\, E\,(\mathrm{GeV})]\}^{1/2}.$$

This expression does not include possible additional effects due to *'Landau' fluctuations* of the energy deposit in the active signal planes, which can be estimated to contribute

$$[\sigma(E)/E]_{Landau} \simeq 3/[\sqrt{N_x} \times \ln(1.3 \times 10^4\,\delta)],$$

where δ (MeV) gives the energy loss per active detector plane. Such additional fluctuations are small for energy losses δ of a few MeV (e.g. a few millimetres of scintillator), but may become comparable to the 'intrinsic' sampling fluctuations for very thin detectors, e.g. gaseous detectors with δ in the keV range. In addition to these 'Landau' fluctuations there is a further source of errors which also depends on the density of the active medium, *'path-length' fluctuation:* low-energy electrons may be multiply scattered into the plane of the active detector and then travel distances much larger than, for example, the gap thickness in gaseous detector planes, depositing considerably more energy compared to that deposited under perpendicular traversal. This effect is quantitatively less significant in dense active layers, because the range of the low energy electrons is comparable to the thickness of these layers. Moreover, increased multiple scattering in dense detector planes will also tend to reduce this effect relative to light absorbers. From Fig. 7 it can be seen that path-length fluctuations may contribute as much as Landau fluctuations to the resolution [14] in detectors with gaseous readouts.

Concluding this section, we compare in Table 2 the measured performance of some characteristic sampling devices, and compare it with the estimated contributions using the formulae given here. The energy resolution is seen to be rather well described by these estimates, provided that instrumental effects (such as calibration errors, photon statistics, leakage, etc.) do not dominate.

It is interesting to note that the path length and the Landau fluctuations are not negligible even in the case of dense active readout gaps, if these are very thin (e.g. measurements with the W/Si calorimeter).

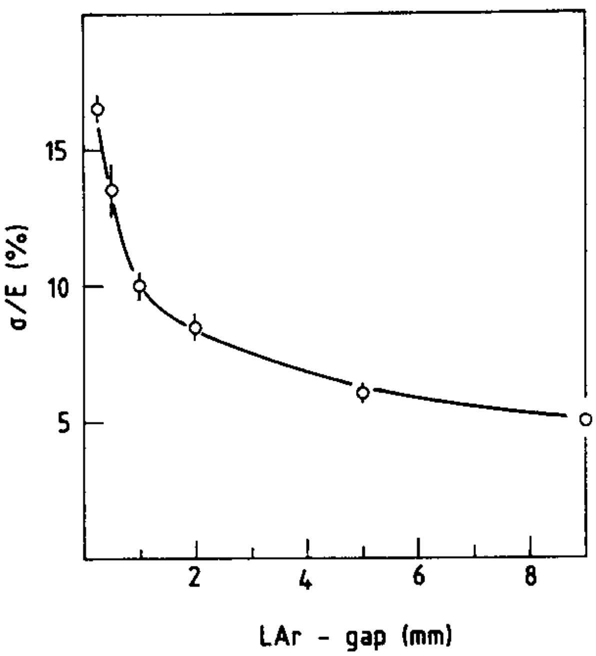

Fig.7a: Energy resolution versus thickness of the active liquid-argon layer for 1 GeV electrons in an iron/argon sampling calorimeter.

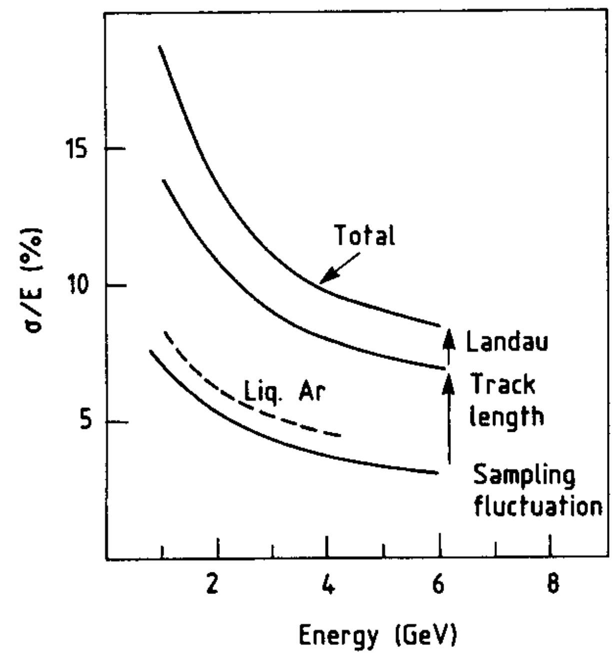

Fig. 7b: Contributions of sampling, path length, and Landau fluctuations to the energy resolution of a lead/MWPC sampling calorimeter. The latter contribute approximately equally ($\sim$ 12% at E = 1 GeV), and combined quadratically with the sampling fluctuations ($\sim$ 7%) they account for the overall resolution of $\sim 18\%/\sqrt{E}$ [14].

Table 2: Measured and Estimated Performance of Electromagnetic Sampling Calorimeters

Device passive/active (mm)	Al/scint. 89/30	Fe/LAr 1.5/2.0	Cu/scint. 5/2.5	W/Si detector 7.0/0.2	$Pb/Ar/CO_2$ at NTP 2.0/10.0	U/scint. 1.6/2.5
Energy resolution measured at 1 GeV(%)	20	7.5	13.0	25.0	$\leq$ 20.0	11.0
η (MeV)	3.0	0.7 (?)	0.7 (?)	0.7 (?)	$\leq$ 0.6 (?)	0.7 (?)
$F(\xi)^{-1/2}$	1.16	1.10	1.10	1.18	1.18	1.20
$\langle\cos\theta\rangle^{-1/2}$	1.00	1.03	1.03	1.27	1.36	1.51
σ^{sample}	23	4.8	9.2	19.1	8.2	10.6
σ_{Landau}	3.8	1.0	1.0	4.5	8.70	1
$\sigma_{\mathrm{path\ length}}$		5.7	6	17.5	13.0	6 (?)
$\sigma_{\mathrm{estimated}}$	23	7.5	10.0	25.9	17.7	12.2
Note	a	b, c	c, d, e	c, f	c, g	c, e, h

a) A.N. Diddens et al., Nucl. Instrum. Methods 178:27 (1980).
b) C.W. Fabjan et al., Nucl. Instrum. Methods 141: 61 (1977).
c) Path-length fluctuations estimated from H.G. Fischer, Nucl. Instrum. Methods 156:81 (1978).
d) O. Botner, Phys. Scripta 23:555 (1981).
e) Difference consistent with photon statistics.
f) G. Barbiellini et al., Nucl. Instrum. Methods 235:55 (1983).
g) J.A. Appel, Fermilab FN-380 (1982).
h) R. Carosi et al., Nucl. Instrum. Methods 219:311 (1984).

2.4 'Transition' Effects

The concept of total track length T has been repeatedly used to estimate properties of the EMC. In particular, it suggests equating the measurable signal in a specific calorimeter with the energy deposit of penetrating particles such as muons of equivalent path length, or in terms of the number of equivalent particles n_{ep}. One equivalent particle (1 ep) is defined as the most probable detected energy, $(dE/dx)^{mp}$ of a penetrating muon

$$1\ \mathrm{ep} = (dE/dx)^{mp}_{\mathrm{visible},\,\mu}\,.$$

The expected number n_{ep} for electrons with kinetic energy E^{el}_{kin} would be

$$n^{el}_{ep}(\mathrm{expected}) = E^{el}_{kin}\,/1\ \mathrm{ep}\,.$$

Experimentally, yet, one always observes:

$$n_{ep}^{el}(\text{visible}) < n_{ep}^{el}(\text{expected}) \quad \text{or} \quad `e/\mu < 1'.$$

A summary of some representative measurements is given in Table 3.

The calibration of an EMC with muons is one way of establishing an absolute energy scale. If carried out in a reproducible and consistent way, it would allow us to compare, on an absolute energy scale, the electron response of different calorimeters—a crucial ingredient also in the understanding of hadronic calorimeters (see Section 3). As an example, the energy scale for muons quoted in Table 3 is based on the most probable

Table 3: Average Calorimeter Response for Pions and Muons*) Relative to Electrons [38]

Type of particle (energy)	Sampling calorimeter structure $\frac{\text{scintillator}}{\text{liquid argon}}$		
	with Fe (Cu)	with Pb	with ^{238}U
Electrons (10 GeV/c)	1	1	1
	1	1	1
Pions (10 GeV/c)	0.63 ± 0.03 [a,b]	0.68 ± 0.04 [b]	0.93 ± 0.03 [b,d]
	0.7 [c]	not yet measured	1.0 ± 0.05 [c]
Muons (~ 10 GeV/c)	1.15 [b]	1.26 [b]	1.29 [b,d]
	1.1	1.4 [e,f]	1.65 [g]

*) See text for definition of muon response.
NB: Errors of typically 10% have to be assumed for figures quoted without error.
a) A. Beer et al., Nucl. Instrum. Methods 224:360 (1984).
b) O. Botner, Phys. Scripta 23:555 (1981).
c) C.W. Fabjan et al., Nucl. Instrum. Methods 141:61 (1977).
d) T. Akesson et al., Properties of a fine-sampling uranium-copper scintillator hadron calorimeter, submitted to Nucl. Instrum. Methods (1985).
e) J. Cobb et al., Nucl. Instrum. Methods 158:93 (1979).
A. Lankford, CERN-EP Internal Report 78-3 (1978).
C. Kourkoumelis, CERN Report 77-06 (1977).
f) P. Steffen (NA31 Collaboration, CERN), private communication.
g) C.W. Fabjan and W. Willis, unpublished note on measurements reported in c).

energy loss evaluated for the total thickness of the device, applying the energy loss formula [15] for the appropriate muon momentum, including the non-negligible relativistic rise. The energy loss in the active medium was estimated to follow the ratio of the respective mass of the passive and active materials. Table 3 shows that the discrepancies from the 'naïve' expectations are substantial, with some indication that the response depends on the sampling thickness and the atomic number of the active and passive materials.

These discrepancies have been repeatedly attributed to 'transition effects' at the boundary between the different layers [16–18], often characterized by very different critical energies and hence different collision losses per radiation length. One expects that at a boundary from high Z to low Z (e.g. Fe to scintillator), the increased collision losses in the low-Z substance will reduce the electron flux, in agreement with measurements [17, 18] and some recent Monte Carlo calculations [19]. Apart from local disturbances of the EMC, multiple scattering tends to increase the effective path length in the high-Z absorber relative to the low-Z readout and this mechanism may also suppress the electron response relative to muons, for increasing Z. Furthermore, a considerable fraction of the energy is deposited by the last generation of the cascade, consisting of low-energy particles, and saturation in the response of readout substances (which occur in scintillator or liquid argon) will further suppress the measured response relative to muons.

It may be concluded that for a more refined understanding of sampling detectors it will be important to calibrate carefully the electron response on an absolute energy scale with a reproducible standard, as provided e.g. by muons.

2.5 Spatial Resolution

In subsection 2.1 we described in general the physical processes contributing to the shower propagation and its characteristic dimension. Typical angles for bremsstrahlung emission and multiple scattering depend on the energy of the shower particles and hence alter the transverse shower profile as a function of longitudinal depth inside the shower. Before the shower maximum, typically more than 90% of the energy is contained in a cylinder of radius $r \simeq 0.5X_0$, whereas the radius for 90% containment of the total energy is $r = 2\varrho_M$. For the localization of the impact point of a photon it is therefore advantageous to probe the shower in the early part before the shower maximum. In principle, given sufficiently fine-grained instrumental resolution, the localization σ_x of the centre of gravity of the transverse distribution is determined by signal/noise considerations and, therefore, should improve with increasing particle energy E as $\sigma_x \sim E^{-1/2}$, which is confirmed experimentally [20], reaching sub-millimetre accuracy for 100 GeV showers [21]. If position resolution is the principal criterion, one may achieve very high spatial subdivision using multiwire proportional chamber (MWPC) techniques [22] allowing localization at the millimetre level.

Somewhat different criteria apply if both good position and energy resolution are required, e.g. for the determination of the invariant mass of particles such as π^0's, $J/\psi \to e^+e^-$, etc. In this case the centres of gravity of the complete showers have to be determined—frequently with the constraint of minimizing the sharing of energy between the neighbouring showers—; even then, excellent spatial resolutions of the order of 1 mm have been reported [20], e.g. in an array of lead-glass blocks of 35 × 35 mm cross-section.

Given simultaneous information on the transverse and longitudinal shower development, the *direction* of a shower and hence the angle of incidence of the particle may be reconstructed. As an example, for the CHARM neutrino calorimeter [23] an angular resolution of $\sigma(\theta_e)$ (mrad) = $20/E^{1/2} + 560/E$ (E in GeV) was measured; for a FNAL neutrino calorimeter [24] the following result is quoted:

$$\sigma(\theta_e)\,(\text{mrad}) = 3.5 + 53/E\,(\text{GeV}).$$

3. HADRONIC SHOWER DETECTORS

3.1 General properties

Conceptually, the energy measurement of hadronic showers is analogous to that of EMCs, but the much greater variety and complexity of the hadronic processes propagating the hadronic cascade (HC) complicate the detailed understanding. No simple analytical description of hadronic showers exists, but the elementary processes are well studied.

Typical of hadronic interactions is multiple particle production with transverse momentum $\langle p_T \rangle \simeq 0.35$ GeV/c, for which about half of the available energy is consumed (the inelasticity $K \simeq 0.5$). The remainder of the energy is carried by fast, forward-going (leading) particles. The secondaries are mostly pions and nucleons, and their multiplicity is only weakly energy-dependent. The characteristic stages in the HC development are summarized in Table 4. Two specific features have been identified as the principal physics limitations to the energy resolution of hadronic calorimeters:

i) A considerable part of the secondaries are π^0's, which will propagate electromagnetically without any further nuclear interactions; the average fraction converted into $f_{\pi^0} \simeq 0.1 \ln E$ (GeV), for energies E in the range of a few to several hundred GeV. The size of the π^0 component is largely determined by the production in the first interaction, and event-by-event fluctuations about the average value are, therefore, important.
ii) A sizeable amount of the available energy is converted into excitation or break-up of the nuclei, of which only a fraction will result in detectable ('visible') energy.

The two processes, intimately correlated, may lead, for a given entering hadron, to a very different shower composition, which has a very different detectable response. Together they impose the intrinsic limitation on the performance of hadronic calorimeters.

Table 4 gives some indications of the relative importance of these competing processes. Considerable insight has been gained from very detailed Monte Carlo calculations, which in their most ambitious form aim to simulate the full nuclear and particle physics aspects of the hadronic cascade based on the measured cross-sections of the elementary processes (see also Section 6) [25]. Examples showing the energy dependence of the principal effects are given in Fig. 8. It should be noted that these various processes contribute in varying degrees to the visible energy of the HC, and that a considerable fraction—such as nuclear binding energy, muons, and neutrinos—will be lost in the form of 'invisible' or undetectable energy.

Table 4: Characteristic Properties of the Hadronic Cascade

Reaction	Properties	Influence on energy resolution	Characteristic time (s)	Characteristic length (g/cm^2)
Hadron production	Multiplicity $\simeq A^{0.1} \ln s$ Inelasticity $\simeq 1/2$	π^0/π^+ ratio Binding energy loss.	10^{-22}	Abs. length $\lambda \simeq 35A^{1/3}$
Nuclear de-excitation	Evaporation energy $\simeq$ 10% Binding energy $\simeq$ 10% Fast neutrons $\simeq$ 40% Fast protons $\simeq$ 40%	Binding energy loss. Poor or different response to n, charged particles, and γ's.	10^{-18}–10^{-13}	Fast neutrons $\lambda_n \simeq 100$ Fast protons $\lambda_p \simeq 20$
Pion and muon decays	Fractional energy of μ's and ν's $\simeq$ 5%	Loss of ν's	10^{-8}–10^{-6}	$\gg \lambda$
Decay of c, b particles produced in multi-TeV cascades	Fractional energy of μ's and ν's at percent level	Loss of ν's. Tails in resolution function.	10^{-12}–10^{-10}	$\ll \lambda$

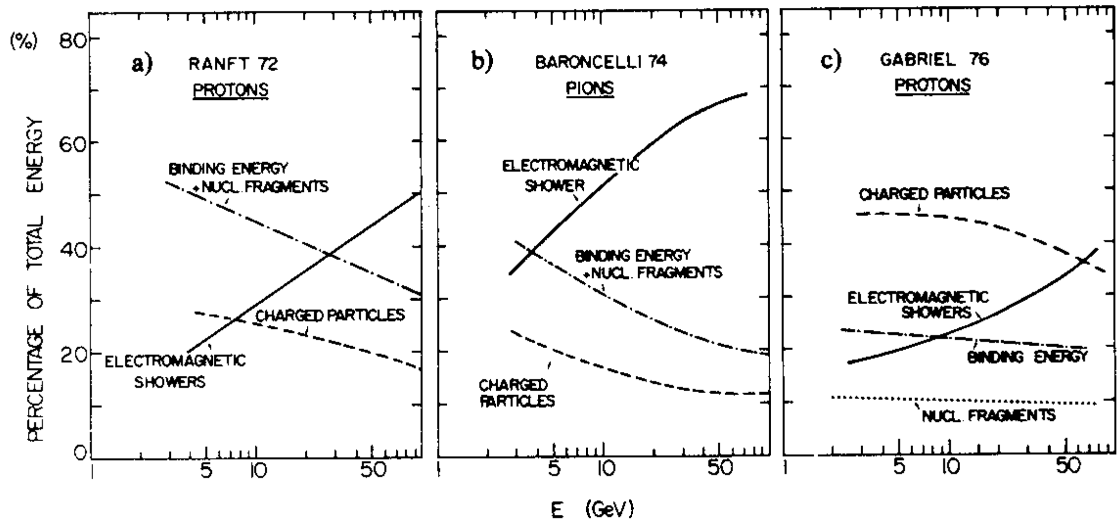

Fig. 8: Relative contributions of the most important processes to the energy dissipated by hadronic showers, as evaluated from three representative Monte Carlo calculations [25].

Average longitudinal and transverse distributions (Fig. 9) are useful estimates of the characteristic dimensions for near-complete shower containment. The average longitudinal distribution exhibits 'scaling in units of absorption length λ'. The transverse distributions depend—as in the case of EMCs—on the longitudinal depth: the core of the shower is rather narrow (FWHM from 0.1 to 0.5λ), increasing with shower depth. The highly energetic, very collimated core is surrounded by lower-energy particles, which extend a considerable distance away from the shower axis, such that for 95% containment a cylinder of radius $R \sim 1\lambda$ is required.

Experimental data are consistent with the following parametrization:

a) the shower maximum, measured from the face of the calorimeter, is given by

$$t_{max}(\lambda) \sim 0.2 \ln E\,(\mathrm{GeV}) + 0.7;$$

it occurs at a smaller depth in high-Z materials due to the smaller ratio of X_0/λ.

b) The longitudinal dimension required for almost full containment is approximated by

$$L_{0.95}(\lambda) \simeq t_{max} + 2.5\,\lambda_{att},$$

again measured from the face of the calorimeter. The quantity λ_{att} describes the exponential decay of the shower beyond t_{max} and increases with energy approximately as $\lambda_{att} \simeq \lambda[E\,(\mathrm{GeV})]^{0.13}$, with an indication of a weaker energy dependence for high-Z absorbers. The expression for $L_{0.95}$ describes available data in the energy range of a few GeV to a few hundred GeV to within 10%.

c) The transverse radius R of the 95%-containment cylinder is very approximately $R_{0.95} \lesssim 1\lambda$; it does not scale with λ and is smaller in high-Z substances.

d) A useful parametrization of the longitudinal shower development is

$$dE/ds = K[wt^a e^{-bt} + (1-w)\,\ell^c e^{-d\ell}],$$

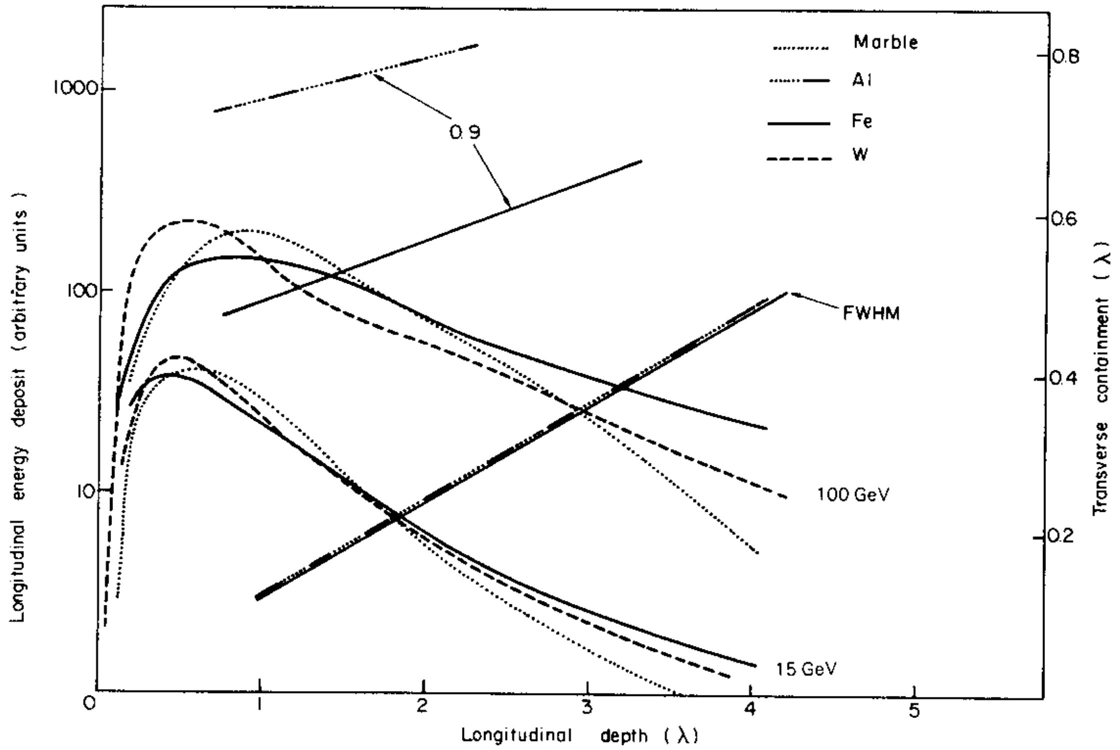

Fig. 9: Longitudinal shower development (left ordinate) induced by hadrons in different materials, showing approximate scaling in absorption length λ. The shower distributions are measured from the vertex of the shower and are therefore more peaked than those measured with respect to the face of the calorimeter. For the transverse distributions as a function of shower depth, scaling in λ is found for the narrow core (FWHM) of the showers. The radius of the cylinder for 90% lateral containment is much larger and does not scale in λ. [10 GeV/c π's: B. Friend et al., Nucl. Instrum. Methods 136:505 (1976)]. Note that marble and aluminium have almost identical absorption and radiation lengths [Marble: M. Jonker et al., Nucl. Instrum. Methods 200:183 (1982); Fe: M. Holder et al., Nucl. Instrum. Methods 151:69 (1978); W: D.L. Cheshire et al., Nucl. Instrum. Methods 141:219 (1977)].

where t is the depth, starting from the shower origin, in radiation lengths, and ℓ is the same depth in units of absorption lengths. The parameters a,b,c,d are fits to the data and are given a logarithmic energy dependence. Crude shower fluctuations may be simulated by i) randomly varying the depth of the shower origin; ii) smearing the incident particle energy to simulate the calorimeter energy resolution; iii) randomly varying the length of the shower by scaling the values of t and l [26].

Although the total depth needed for near-complete absorption increases only logarithmically with energy, it does require, for example, about 8λ to contain, on the average, more than 95% of a 350 GeV pion.

3.2 Intrinsic Energy Resolution

In the previous subsection we indicated that the fluctuations in the HC development, producing a range of different particles—from π^0's to slow neutrons, muons, and neutrinos—with vastly different detection characteristics, are the principal limitations to the energy resolution. These fluctuations have been found to be large—of the order of 50% at 1 GeV—in strong contrast with the measurement of e.m. calorimeters, where the *intrinsic* fluctuations of the visible track length are less than 1% at 1 GeV. This understanding of hadronic cascades emerged from studies in which the various possible contributions could be individually identified and measured [27]. The dominant influence of the nuclear processes manifests itself also in the shape of the response function (Fig. 10) and is corroborated by detailed Monte Carlo estimates. Available experimental evidence indicates that the intrinsic hadronic energy resolution is

$$\sigma(E)/E|_{\mathrm{intrinsic}} \simeq 0.45/\sqrt{E}\ (\mathrm{GeV})\,.$$

This relation describes devices made from materials covering almost the complete periodic table from aluminium [23] to lead [28]. Only in hydrogen are these nuclear effects absent, but they are already sizeable in hydrogen-rich absorbers (e.g. scintillators): one measurement in an homogeneous liquid-scintillator calorimeter is reported [29] for which the quoted energy resolution is also consistent with the above-quoted value. The sole known exception from this rule is given by uranium-238, for reasons that are explained in the next subsection.

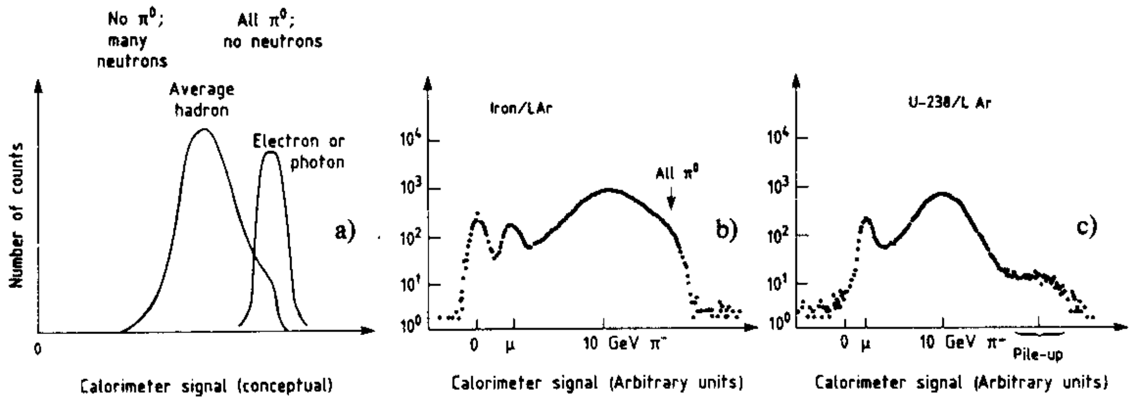

Fig. 10: Calorimeter response for 10 GeV/c pions.
a) Conceptually, the fluctuations are dominated by the nature of the first inelastic interaction. On the average, a certain number of π^0's, charged pions, nuclear fragments, and slow protons and neutrons will be produced. In one extreme case, no π^0's will be produced—only charged pions, neutrons, etc. (low-energy side of response function). At the other extreme the reaction products are mostly π^0's, and the energy deposit will be very similar to that of electrons or photons of equivalent energy.
b) The measured response function is shown for a calorimeter using iron as absorber. The logarithmic ordinate exposes a break in the resolution function corresponding to the case of mostly electromagnetic propagation.
c) The response for a U-238 sampling calorimeter is shown. The nuclear losses are effectively compensated, leading to a response that is nearly equal for charged and neutral pions. The essentially Gaussian response function is also an indication of this uniform response. (The muon peak sets the energy scale corresponding to 'one equivalent particle').

The level of these nuclear effects and, more generally, the level of 'invisible' energy is sensitively measured by comparing the response of a calorimeter for electrons and hadrons at the same 'available' energy, which is the kinetic energy of electrons and nucleons, the total energy for mesons, and the total energy plus the rest mass for antinucleons. A summary of some representative data is shown in Fig. 11. Two features deserve a comment: all calorimeters except those made from uranium show a visible energy of approximately 70% relative to electrons, which slowly increases owing to the rise in the electromagnetic component at higher energies. On the other hand, with energies decreasing below E ~ 1.5 GeV, the nature of the hadronic cascade changes: to a larger measure, the energy is degraded by ionization alone, with the hadron response approaching that of muons and being above that of electrons (see subsection 2.4). In this low-energy limit all calorimeters, including those using uranium as a degrader, are expected to give similar responses. This interpretation is confirmed by the fact that in this low-energy regime the relative resolution improves, $\sigma/E < 0.45/\sqrt{E}$ [30–32], as well as by quantitative Monte Carlo estimates [32].

In summary, the response of hadrons relative to electrons is a sensitive probe of the level of nuclear effects. Typical values are $e/h \simeq 1.4$ for most materials. Strongly correlated with this average suppression are fluctuations in the response; these are due to large fluctuations of the electromagnetic component. The intrinsic resolution of hadron calorimeters is, for these reasons, limited to $\sigma(E)/E_{intrinsic} \simeq 0.45/\sqrt{E}$ (GeV), unless event-to-event fluctuations in the electromagnetic component of hadron cascades are somehow corrected for. This applies likewise to *homogeneous* and *sampling* devices.

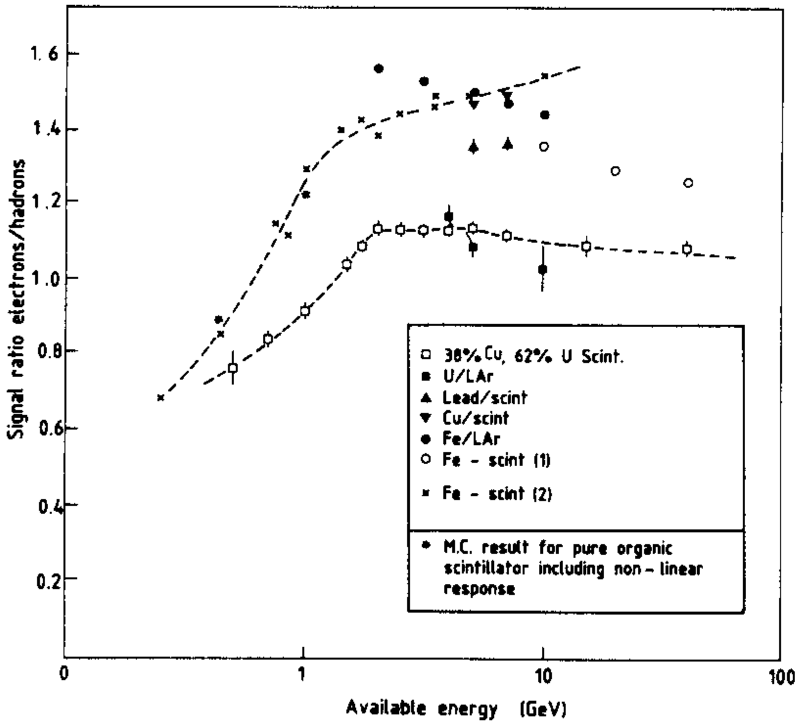

Fig. 11: The ratio of electromagnetic to hadronic energy response as a function of energy for different calorimeter systems: 38% Cu, 62% U/scint. [32]; U/LAr [37]; Cu/scint. [88]; Fe/LAr [37]; Fe/scint. (1) [35]; Fe/scint. (2) [31].

3.3 Compensating Fluctuations

We have emphasized that the relative response between electrons and pions is a sensitive measure of the level of nuclear interactions. An improvement in the energy resolution would be expected if the response of the electromagnetic cascade were identical compared with the purely hadronic one, i.e. if devices with an e/h ratio equal to one were available. Alternatively, given sufficiently detailed information on the individual hadronically induced shower, one would be able to assess the relative components and apply suitable corrections to improve the energy resolution. Both approaches have been explored and are described here.

Several suggestions have been made for monitoring the level of the electromagnetic component event-by-event. One suggestion was to use, as an indicator, the Cherenkov light from relativistic particles dominantly produced by e^+e^- pairs [33], but Monte Carlo estimates [33] for practical devices suggest that it is difficult to obtain a very useful correlation and to improve the resolution significantly. Another suggestion was to monitor the level of the nuclear component by associating heavily ionizing particles with the 'late' component of the hadronic shower [34]. If a calorimeter is instrumented so as to provide detailed longitudinal information, then some useful compensation on a shower-by-shower basis is possible for the electromagnetic/hadronic fluctuations. The most successful attempt was made by the CERN-Dortmund-Heidelberg-Saclay (CDHS) collaboration using the longitudinal information from their relatively fine-grained neutrino calorimeter [35, 36]. This was done by a weighting algorithm applied to the individual longitudinal measurements relative to the total energy measured. In Fig. 12 the unweighted and weighted results for the energy resolution are presented. Firstly, it can be seen that the raw results show a marked deviation from the expected $E^{-1/2}$ dependence.

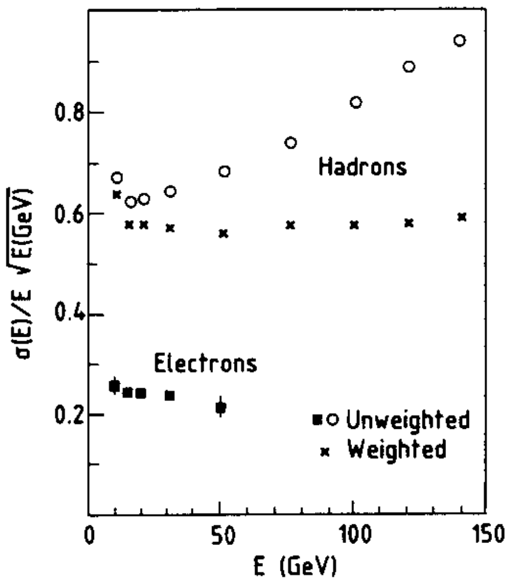

Fig. 12: Energy resolution measured in the CDHS neutrino calorimeter (2.5 cm Fe/scint.) versus the energy of the incident particle. Note that the uncorrected energy resolution for hadrons does not improve as $1/\sqrt{E}$. With a weighting procedure to reduce the large fluctuation due to the e.m. component the resolution is improved, and is consistent with the $1/\sqrt{E}$ scaling up to the highest energies measured [35].

This cannot be ascribed to instrumental effects given the reported result for the electron resolution, which is well described by an $E^{-1/2}$ law. Secondly, the weighting algorithm improves the resolution, particularly at the highest energies, to a level that would be expected from extrapolating the low-energy resolution according to an $E^{-1/2}$ law. In subsection 3.5 we comment further about this deviation from the naïve $1/\sqrt{E}$ behaviour of hadronic calorimeters at high energies.

The more direct cure for these fluctuations would be to equalize the response for electrons and hadrons. In principle, equalizations of these differences, which are at the 30% to 40% level, may be accomplished in two ways: either by decreasing the electron response—typically 20% to 40% lower relative to a minimum-ionizing particle calibration (subsection 2.2); or by boosting the hadronic signal. This latter aspect is being exploited by using uranium-238 as the energy degrader [37]. In that material (and probably also to a lesser extent in thorium) some of the normally invisible energy expended in the nuclear break-up leads to neutron-induced fission, which in turn produces detectable energy in the calorimeter. It can be estimated that on the average 40 fissions are induced per GeV of energy deposited, which altogether liberate about 10 GeV of fission energy. Only a very small fraction (300 to 400 MeV) needs to be detected in order to compensate the nuclear deficit; this could be done either by the few-MeV γ-component or through the fission neutrons liberated in the fission process. Which component and what fraction of the fission contributions are measured depends on the nature of the active sampler. One may achieve essentially complete compensation not only on average but also event-by-event, because the intrinsic resolution is measured to be [32, 37]

$$\sigma(E)^{\text{uranium}}_{\text{intrinsic}} \simeq 0.22/\sqrt{E}\ (\text{GeV}) .$$

The fundamental importance of equalizing the hadronic and electromagnetic response should again be emphasized. The latter sensitively depends on the details of the low-energy part of the EMC and hence critically on the material and the sampling frequency. It would appear that this is one further contribution to the tuning of the e/h ratio. Hence for hadron showers, the level of visible compensation is expected to be affected not only by the choice of the passive absorber but also by the response of the active readout to densely ionizing particles (from the HC) and to the electromagnetic component. We do not yet have a complete set of measurements, but Table 3 attempts to organize the available information [38].

3.4 Instrumental Effects to the Energy Resolution

Most hadronic calorimeters are 'sampling' detectors, using preferentially rather dense passive absorbers to reduce the linear dimensions of the instrument. As a consequence, sampling fluctuations of statistical origin analogous to the case of electromagnetic sampling fluctuations (section 2.3) may contribute to the energy resolution, although, for the sampling of the HC we do not have a similar detailed description. Available measurements (see Fig. 13 with the quoted references) are consistent with a parametrization of the form

$$\sigma(E)/E/\text{hadron-sampling} \simeq 0.09\ [\Delta E\ (\text{MeV})/E\ (\text{GeV})]^{1/2} .$$

The quantity ΔE expresses the energy loss per unit sampling cell for minimum ionizing particles. Hadronic sampling fluctuations are approximately twice as large as the

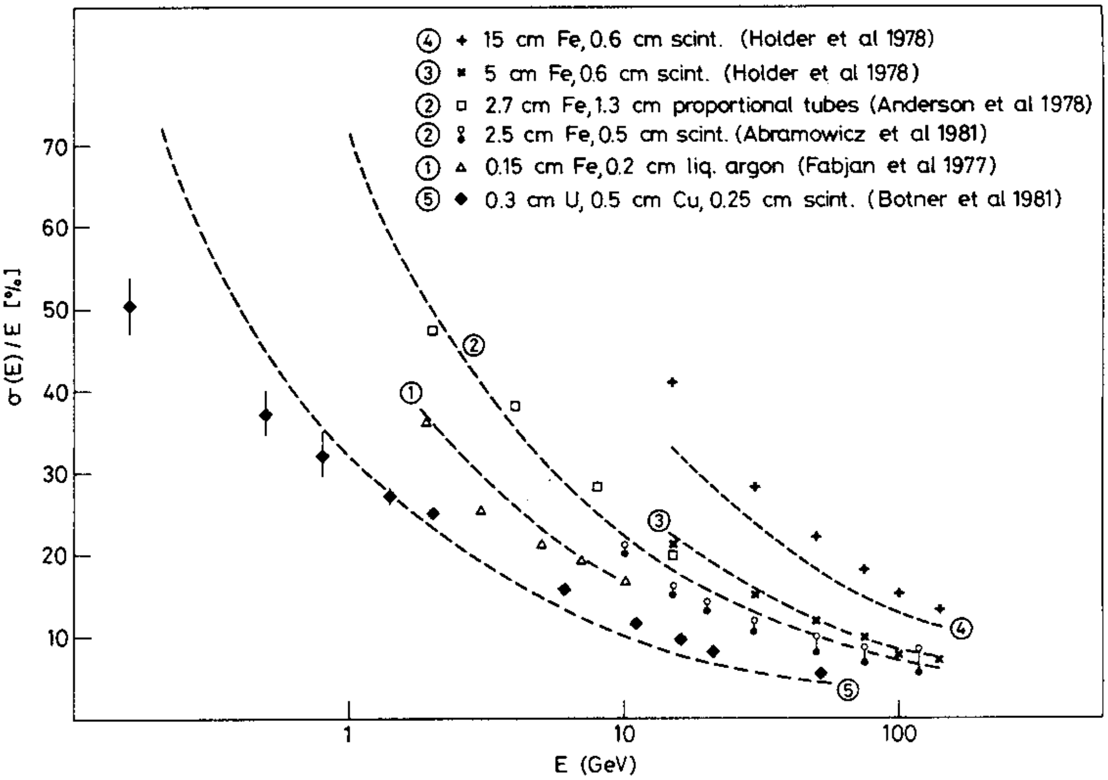

Fig. 13: Energy resolution for hadrons measured with iron and uranium sampling calorimeters. Curves 1–4 are calculated with the values for intrinsic and sampling fluctuations as given in Table 5. For the data on curve 2 [35], the open circles are the raw data; the solid circles are the results of the off-line analysis, using the longitudinal shower information to correct for fluctuations in the electromagnetic/hadronic energy ratio. For curve 5 the intrinsic fluctuation is assumed to be $0.2/\sqrt{E}$, and does not take account of the 35% (in units of λ) admixture of Cu. Below 1 GeV the resolution improves over the expected value and indicates the influence of mechanisms such as ranging and reduced nuclear effects [32, 88]. The data labelled 3 and 4 are by M. Holder et al., Nucl. Instrum. Methods 151:69 (1978), the open squares refer to R.L. Anderson et al., IEEE Trans. Nucl. Sci. NS-25:1-340 (1978).

electromagnetic sampling fluctuations for the same detector; unlike the e.m. case however, where sampling is the predominant contribution to the resolution, sampling in hadronic detectors can be made small relative to the large intrinsic component, and energy resolution need not be sacrificed in hadronic sampling calorimeters.

Energy leakage due to partial shower containment will not only degrade the energy resolution, but will also give rise to very asymmetric resolution functions with low-energy tails. Calorimetric experiments, which emphasize measurements such as neutrino detection based on missing energy or hadronic high-p_T jet production have therefore particularly stringent requirements to achieve very close to 100% containment. Again, as already noted for the measurement of e.m. calorimeters, longitudinal fluctuations are larger than transverse fluctuations and hence longitudinal leakage is more critical to the performance. For values of fractional leakage f $\leq$ 0.3 the degradation of the energy resolution follows approximately the expression

$$\sigma(E)/E \simeq [\sigma(E)/E]_{f=0} \times (1+4f)\,,$$

with the effect being somewhat more pronounced at higher energies for a given fractional energy leakage.

3.5 Calorimetric Energy Resolution of Jets

Increasingly, the physics emphasis is shifting from the measurement of single particles to the analysis of jets of hadrons considered as the principal manifestation of quarks and gluons. This trend is expected to be pursued at the future multi-TeV hadron colliders, where the spectroscopy of particles in the 100 to 1000 GeV range will largely be done through the invariant mass determination of multijet systems [39]. There are two distinct contributions to the resolution of this invariant mass determination. The first effect is associated with the physics of jet production. Jets, unlike single particles, are not unambiguously defined objects, but have to be defined operationally by a 'jet algorithm' (Fig. 14). For example, hadron-initiated jets are produced together with particles originating from peripheral interactions; multijets may partially coalesce. The second contribution to the mass resolution depends on the calorimeter performance itself, and in particular on the momentum response to different particles (Fig. 11). This is seen conceptually in Fig. 15 for two different calorimeters, which have rather comparable nominal resolutions but a very different response to electrons and pions. For very low

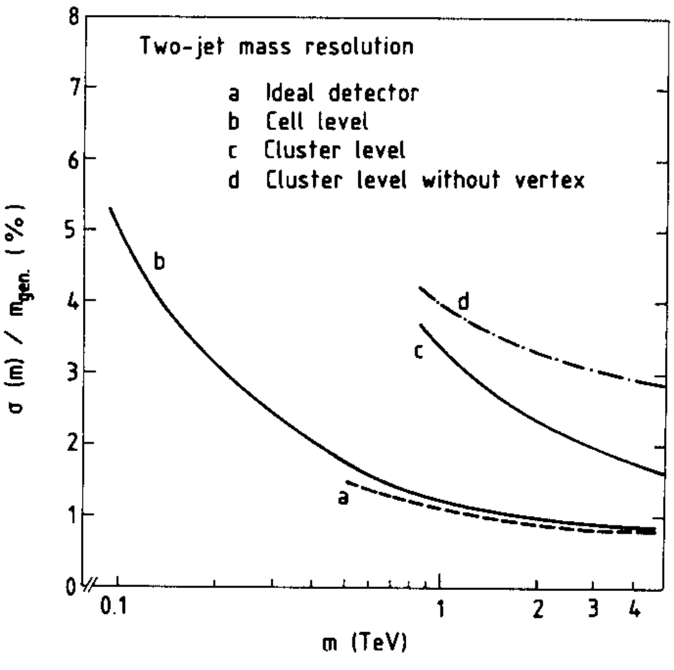

Fig. 14: Two-jet mass resolution as a function of the two-jet mass and for various assumptions on the detector performance. The ideal detector measures the jet mass at the individual particle level; at the cell level the energy information from each cell ($\Delta\phi \times \Delta\eta = 5° \times 0.05$) is considered. At the 'cluster level' certain pattern recognition criteria are introduced. Precise knowledge of the event vertex is important [39].

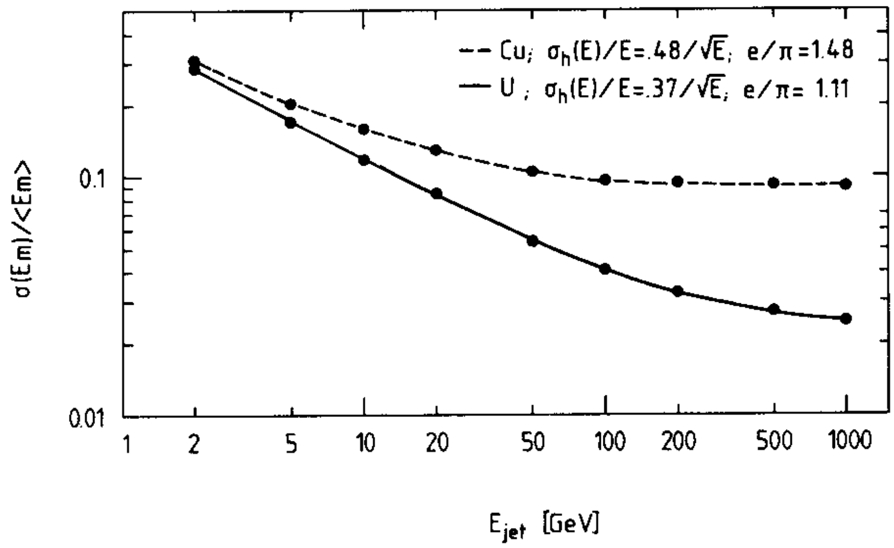

Fig. 15: Jet resolution for an 'infinitely' thick, 4π calorimeter, assuming a Feyman-Field-like fragmentation function. The advantage of a (nearly) compensated calorimeter is particularly evident at very large jet energies. For calorimeters with e/h very different from one, the resolution ceases to improve as $E^{-1/2}$ in the high-energy limit [39].

energies of the jets ($E_{jet} \leq 5$ GeV), the jet resolution is dominated by the very non-linear response to low-momentum particles, and is similar for both calorimeters. At very high energies, the performance is dominated by the relative electron/hadron response. In particular, for the e/h = 1.48 calorimeter it is estimated that the energy resolution levels at approximately 10%. Qualitatively, such a strong influence is expected, because a large fraction of the jet energy is carried by only a few high-momentum particles; fluctuations in the charged hadron/π^0 ratio of these leading particles at sufficiently high energies will dominate over the simple statistical $E^{-1/2}$ improvement.

A similar argument should also be valid for single, very energetic hadrons, which after the first inelastic interaction in a calorimeter will be similar to a jet of particles of comparable energy. Therefore, hadron calorimeters with e/h $\neq$ 1 are expected to show an intrinsic energy resolution $\sigma(E)/E \sim c \times E^{-\alpha}$, with $\alpha < 1/2$ for large energies ($E > 50$ GeV). This behaviour is consistent with the careful analysis (Refs. [35, 36], and Fig. 12) discussed in the previous subsection. Table 5 summarizes the contributions to the energy resolution for both electromagnetic and hadronic calorimeters.

3.6 Spatial Resolution for Hadronic Showers

This discussion follows closely the related comments on e.m. calorimeters (subsection 2.5). Hadron showers are found to consist of a narrow core surrounded by a 'halo' of particles extending to several times the dimensions of the core. Consequently, somewhat different criteria apply to the measurement of the position and to considerations of shower separation. Measurements on the spatial resolution of the impact point [23, 32] may be parametrized approximately in the form

$$\sigma(\text{vertex})\ (\text{cm}) \simeq \langle\lambda\rangle/[4\sqrt{E}\ (\text{GeV})]\,.$$

Table 5: Principal Contributions to Energy Resolution in Electromagnetic and Hadronic Calorimeters

Mechanisms (add in quadrature)	Electromagnetic showers	Hadronic showers
Intrinsic shower fluctuations	Track-length fluctuations: $\sigma/E \gtrsim 0.005/\sqrt{E}$ (GeV).	Fluctuations in the energy loss: $\sigma/E \simeq 0.45/\sqrt{E}$ (GeV). Scaling weaker than $1/\sqrt{E}$ for high energies. With compensation for nuclear effects: $\sigma/E \simeq 0.22/\sqrt{E}$ (GeV).
Sampling fluctuations	$\sigma/E \simeq 0.04\sqrt{\Delta E/E}$. Nature of readout may augment sampling fluctuations.	$\sigma/E \simeq 0.09\sqrt{\Delta E/E}$
Instrumental effects	Noise and pedestal width: $\sigma/E \sim 1/E$ - determine minimum detectable signal; - limit low-energy performance. Calibration errors and non-uniformities: $\sigma/E \sim$ constant and therefore limits high-energy performance.	
Incomplete containment of shower	$\sigma/E \sim E^{-\alpha}$, $\alpha < 1/2$ (see subsec. 2.2, resp. 3.4). For leakage fraction $\geq$ few ‰: non-linear response and non-Gaussian 'tail'.	

a) $\Delta E \simeq$ energy loss of a minimum ionizing particle in one sampling layer, measured in MeV; E = total energy, measured in GeV.

In compact calorimeters, where the average interaction length may be as low as $\langle\lambda\rangle \leq 20$ cm, spatial resolutions in the range of a few centimetres at 1 GeV are achievable. The influence of the transverse segmentation has also been studied [40] and the following dependence can be derived:

$$\sigma(\text{vertex}) \simeq \sigma_0\,(\text{vertex})\exp(2d)\,,$$

where the segmentation d is expressed in units of absorption length and σ_0 refers to the intrinsic vertex resolution in the absence of instrumental effects due to finite segmentation. This expression suggests that the improvement becomes rather modest if the lateral segmentation is increased beyond $d\langle\lambda\rangle \leq 0.1$, even disregarding other aspects such as photon statistics or noise.

Finally, the angular resolution of hadron showers has been carefully studied for several calorimeters used to investigate neutrino scattering. The limitations again stem from fluctuations in the $\pi^{\pm}/\pi^0$ composition of the HC, because of their (usually) very different spatial shower developments. These effects were purposely minimized in the case of the CERN-Hamburg-Amsterdam-Rome-Moscow (CHARM) neutrino calorimeter with the choice of marble as the passive absorber material in which EMCs and HCs have approximately the same dimensions [$3X_0$ (cm) $\sim \lambda$ (cm)]. An angular resolution of

$$\sigma(\theta)_{\mathrm{hadron}}\,(\mathrm{mrad}) \simeq 160/\sqrt{E\,(\mathrm{GeV})} + 560/E\,(\mathrm{GeV})$$

is reported [23], and a similar result was obtained with a detector constructed for the same purpose at FNAL [24].

4. PARTICLE IDENTIFICATION

With hadronic calorimeters it is possible to identify a class of particles which are not always easily identified by other methods, and which may be particularly interesting for very topical physics studies, as summarized in Table 6.

In the following, we discuss in some detail the identification of electrons, muons, and neutrinos.

Table 6: Particle Identification with Calorimeters

Particle produced	Calorimeter technique	Comment
Electron, e	Charged particle initiating the electromagnetic shower	Background from charge exchange $\pi^{\pm} N \rightarrow \pi^0 + X$ in calorimeter; π discrimination of $\sim$ 10–1000 possible
Photon, γ	Neutral particle initiating the electromagnetic shower	Background from photons from meson decays
$\pi^0, \eta, \ldots \rightarrow \gamma\gamma$ $\varrho, \phi, J/\psi, \Upsilon, \ldots$ $\rightarrow e^+e^-$	Invariant mass obtained from measurement of energy and angle	Classical application for electromagnetic calorimeters;
Protons, deuterons, tritons, ... and their antiparticles	Comparison of visible energy E_{vis} in calorimeter with momentum of particle	$E_{vis}^{b(\bar{b})} = (\vec{p}_b^{\,2} + m_b^2)^{1/2} - (+)\, m_b$ Protons (antiprotons) identified up to 4 (5) GeV/c; deuterons (antideuterons) correspondingly higher
(Anti)neutrino	Visible energy E_{vis} in calorimeter compared with missing momentum	Important tool for $e^+e^- \rightarrow \nu(\bar{\nu}) + X$ and at CERN Collider (FNAL $p\bar{p}$ collider, $pp(p\bar{p}) \rightarrow \nu(\bar{\nu}) + X$
Muon	Particle interacting only electromagnetically (range). E_{vis} compared to $\vec{p}$.	Background from non-interacting pions
Neutron or $K_L^0(\bar{n}, \bar{K}_L^0)$	Neutral particle initiating hadronic shower	Some discrimination perhaps possible based on detailed (longitudinal) shower information

4.1 Discrimination between Electrons (Photons) and Hadrons

The discrimination is based on the difference in the shower profiles, accentuated in materials with very different radiation and absorption lengths. One finds approximately

$$\lambda\,(\mathrm{g/cm^2})/X_0\,(\mathrm{g/cm^2}) \sim 35A^{1/3}\,Z^2/180A \sim 0.12Z^{4/3},$$

which explains that heavy materials (lead, tungsten, or uranium) are best suited for electron–hadron discrimination.

The principal physics limitation is imposed by the charge exchange reaction $\pi^-p \to \pi^0 n$ (or $\pi^+ n \to \pi^0 p$), which may, under unfavourable circumstances, simulate an electromagnetic shower, closely matching the energy of the incident pion. For pion energies in the few-GeV range, the cross-section for this process is at the one percent level of the total inelastic cross-section, and decreases logarithmically with energy [41]. Typical values for pion discrimination are of the order of 1 in 10^2 in the 1 to 10 GeV region and of 1 in 10^3 or more for particles energies beyond 100 GeV [42]. Considerably better performance (close to 10^3 pion rejection for few-GeV particles) is reported for instruments with very fine longitudinal subdivision [43], which helps to recognize the hadronic origin of a charge-exchange-dominated cascade. Only relatively small further improvements (a factor of 3 to 5) are obtained if transverse shower profile information is available; this is because of the very high degree of correlation between transverse and longitudinal profile [44, 45]. The quoted values apply to electron–hadron discrimination based on shower shape analysis only. If, in addition, energy information can be used, for example knowledge of the electron and pion momenta from magnetic spectroscopy, a further improvement in the rejection of typically one order of magnitude is obtained.

4.2 Muon Identification

Several calorimetric methods exist for discriminating between muons and hadrons or electrons, all based on the very large differences of energy deposit.

i) Calorimeters with fine longitudinal subdivision: such calorimeters, typically many tens of absorption lengths long, have been used predominantly in experiments on incident neutrinos. Energetic muons are very clearly recognized as isolated, minimum-ionizing tracks, frequently ranging far beyond the tracks from hadronic showers.
ii) Muon penetration through active or passive absorbers: the absorbers or calorimeters are deep enough to contain the hadrons adequately and to reduce the 'punch through' probability P of pions ($P \sim e^{-d/\langle\lambda\rangle}$). The observed path length d is measured in units of 'detectable' absorption lengths $\langle\lambda\rangle$, which is found to agree closely with tabulated values [46]. The detailed rejection power against hadrons depends critically on the experimental precautions taken and may be improved by
a) reducing the background from pion and K decay before the calorimeter; the active 'beam dump' experiments have refined this method [47];
b) measuring the muon momentum after the calorimeter in, for example, magnetized iron [48] or a precision magnetic spectrometer [49]; momentum matching of muon candidates before and after the absorber may further improve the rejection [50];
c) correlating the direction of the particle before and behind the absorber. The applicability of the method is limited by multiple scattering of the muons in the absorber (Fig. 16), and accidental overlap with nearby tracks before the absorber.

Very good muon identification will be of increasing importance for experimentation at the storage rings under construction [the FNAL 2 TeV $p\bar{p}$ collider, the CERN Large Electron-Positron Storage Ring (LEP)], or *a fortiori* at those being discussed [the Superconducting Super Collider (SSC) in the USA, the Large Hadron Collider (LHC) in the LEP tunnel]. The very high particle density will make the identification of electrons inside jets extremely difficult, leaving possibly only the muon as a charged lepton signature. In addition, accurate momentum measurement of the muon will be inevitable

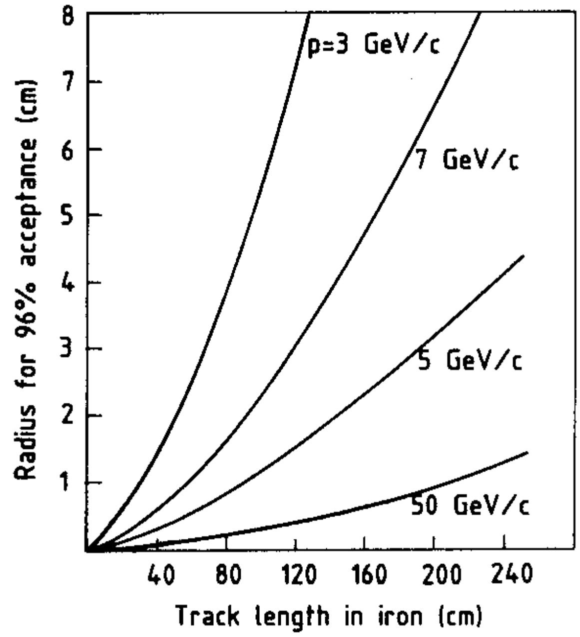

Fig. 16: Radius of 96% acceptance circle for multiply scattered muons as a function of muon track length in iron and of muon momentum. [H. Burmeister et al., CERN/TCL/Int. 74-7 (1974)].

for those experiments which will increasingly exploit very good total energy measurement, for which, of course, the muon momentum has to be included [50, 51].

4.3 Neutrino Identification

The recent discovery of W production based on 'missing momentum' analysis [52] has reminded us of the power of such information. Two related methods can be used:

i) total energy measurement can be accomplished provided 4π calorimetric coverage in the c.m. system is available for all particles (charged, neutrals, muons). This can be practically achieved at e^+e^- storage rings (although 4π hadron calorimetry is not the forte of the forthcoming LEP experiments) or in a fixed-target environment [50]. Neutrino production is implied whenever the measured energy is lower than the total available energy and incompatible with the resolution function of the detector. Total energy measurement does not work well at a hadron collider, such as the CERN $p\bar{p}$ Collider, because a significant fraction of the total energy is always produced at very small angles relative to the incident beams, making a calorimetric measurement impractical. Fortunately, help is provided by

ii) a missing transverse momentum measurement. In this method, clearly related to method (i), the production of a neutrino is signalled by $\Sigma p_{T,i} \neq 0$ to a degree which is incompatible with the detector resolution. Very good missing-momentum resolution at the level of $\sigma(p_{T,miss})/p_{total} \gtrsim 0.3/\sqrt{E}$ has been estimated [53]. This is to be contrasted with the actual performance of a much cruder device for which a $\sigma(p_{T,miss}) \sim 0.7\sqrt{p_T}$ (GeV) is quoted, which is still adequate for a range of striking experimental results [52].

5. SIGNAL READOUT TECHNIQUES FOR CALORIMETERS

During the last 10 years, considerable effort has been devoted to calorimeter instrumentation with a view to developing readout techniques which optimally match an experimental application. The principal goal is to develop methods which will minimize the instrumental effects, relative to the intrinsic performance, caused by the physics of the detectors. Modern beam facilities with their steadily increasing particle energies impose ever more taxing criteria:

- the response must be linear as a function of the particle energy, frequently over a very large dynamic range; only for the exceptional case of energy measurement on isolated particles is a non-linear response acceptable, because it could be remedied (in principle) by calibration;
- the 'noise' or the non-uniformity of the readout system (photoelectron statistics, equivalent noise charge of preamplifiers) must not dominate the energy resolution;
- the readout system must have a rate capability adapted to the observed interaction rate;
- provision must be made for adequate longitudinal and transverse segmentation;
- the absolute and relative energy response must be monitored and maintained with sufficient accuracy;
- other operational characteristics, such as sensitivity to magnetic fields, radiation and temperature, have to be considered.

We have already emphasized the fundamental distinction between homogeneously active or sampling devices. The former have been used in many practical applications for the measurement of electromagnetic showers, whilst the latter represent the only really practical form of hadronic calorimeters. The instrumentation used can be categorized as 'light-collecting' devices measuring scintillator or Cherenkov light or as 'charge-collecting' methods, operating in the ion chamber, proportional, streamer, or saturated Geiger modes. In the following discussion, only recent developments or novel applications are emphasized, as witnessed by the choice of a very restricted number of references from the vast amount of literature.

5.1 Homogeneous Calorimeters

Some of the active readout materials have a density that is high enough for them to be used as homogeneously sensitive calorimeters. The properties of most frequently used materials are summarized in Table 7 [54–79].

Among recent noteworthy developments we find:
- a programme to use BGO crystals (amongst the presently known, optically transparent materials, the one with the shortest radiation length) for large 4π photon calorimeters with excellent space and energy resolution [49, 61];
- materials with considerably improved radiation resistance [64, 65, 74, 75];
- the use of BaF_2 crystals, coupled to very fast UV-sensitive light detectors for very high rate applications [73, 74].

5.2 Readout systems for sampling calorimeters

A great and very diversified number of readout systems have been developed, reflecting the desire to tailor the systems performance to a physics application.

Table 7: Properties and Performances of Homogeneous e.m. Shower Detectors

Detector type	NaI(Tl)	CsI(Tl)	BaF_2	$Bi_4Ge_3O_{12}$	Scintillating glass	Lead glass 55% PbO + 45% SiO_2	$Tl(HCO_2)$-liquid 'Helicon'	Liquid argon
Radiation length (cm)	2.59	1.86	2.1	1.12	~ 4	2.36	~ 1.9	14
Density (g/cm^3)	3.7	4.51	4.9	7.13	~ 3.5	4.08	~ 4.3	1.4
Detection mechanism	Scintillation	Scintillation	Scintillation (20% around 210 nm, 80% around 310 nm)	Scintillation	Scintillation	Cherenkov light	Cherenkov light	Ionization charge
Energy resolution (E in GeV)	$\sim 0.015\ E^{-1/2} < 1$ $< 0.015\ E^{-1/4} > 1$	Comparable to NaI(Tl)	Comparable to NaI(Tl)	Comparable to NaI(Tl)	$\sim 0.002\ E^{-1/2}$	$\sim 0.04\ E^{-1/2}$	Comparable to lead glass	$\gtrsim 0.02\ E^{-1/2}$
Principal limitation to $\sigma(E)$	Shower fluctuations optically non-uniform	Similar to NaI(Tl)	Light collection non-uniformities	Similar to NaI(Tl)	Photon statistics	Photon statistics	Photon statistics	Effect of shower fluctuation on electron collection
Signal[a] (photo-el/GeV)	$\sim 10^7$	$\sim 5 \times 10^6$	$\sim 10^6$	$\sim 10^6$	Few $\times 10^3$	10^3	$\leq 10^3$ (?)	$\leq 2 \times 10^6$
Characteristic time (ns)	250	900	0.6 ; 300	350	~ 70	~ 20	~ 20	≥ 100
Rad. damage at appr. dose[b] (Gy)	$\leqslant 10$	$\leqslant 10$	$\sim 10^5$	~ 10	$\sim 10^4$	$\sim 10^2$	$\geq 10^4$	Not measured; expected to be very large
Mechanical stability	Hygroscopic, fragile	Very good	Good	Good	Very good	Very good	Toxic liquid	Cryogenic liquid
References	[54, 55, 57]	[72]	[73, 74]	[61–63]	[64, 65]	[66–69]	[75]	[76–79]

a) Values are approximate, and depend on spectral matching between light source and photon detector.
b) Values are guidelines only and very substantially depending on experiment and measuring conditions.

5.2.1 Light-collecting sampling calorimeters. The renaissance of such calorimeters started with the introduction of cheap 'plastic scintillators' and elegant light-readout techniques using 'wavelength shifters' (WLSs) to replace the technique of scintillator plates individually coupled to a lightguide [80] (Fig. 17a). The principle is indicated in Fig.17b [81–89]. Scintillation light crosses an air gap and enters the WLS, where it is absorbed and subsequently re-emitted at longer wavelengths; a fraction of this 'wavelength shifted' light is then internally reflected to the light detector. This scheme avoids complicated and costly optical contacts between the scintillators and the light collectors, and minimizes dead spaces. A variety of scintillators have been developed for the large calorimeter facilities. They are based on polymethyl methacrylate (PMMA) [90] or polystyrene [30] as the matrix for the primary scintillating agent. The light yield is close to that of more conventional organic scintillators (usually based on a polyvinyl toluene solvent) if certain aromatic compounds, e.g. up to about 20% naphthalene, are added. These new scintillators are more easily mass-produced, hence cheaper, and have superior mechanical properties. Some of the limitations of the WLS method may be removed after further development: better spectral matching between the scintillator emission and the WLS absorption, and also between the WLS emission and the photocathode sensitivity, will increase the number of detected photons, which is marginal in present systems. Related developments might result in the use of thinner yet more uniform WLSs; increased granularity might be achieved with WLSs having spatially

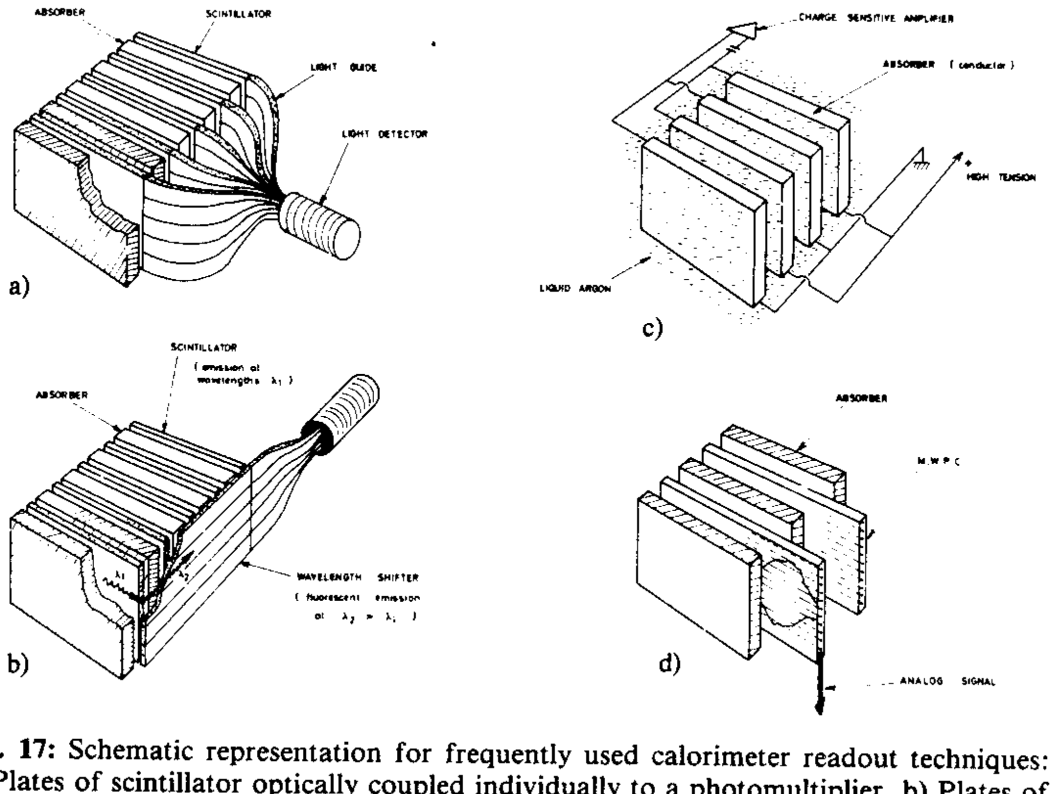

Fig. 17: Schematic representation for frequently used calorimeter readout techniques: a) Plates of scintillator optically coupled individually to a photomultiplier. b) Plates of scintillator read out by photon absorption and conversion in a wavelength shifter plate. c) Charge produced in an electron-transporting medium (e.g. liquefied or high-pressure argon) collected at electrodes, which may also function as the passive absorber plates. d) Charge produced in a proportional gas and amplified internally on suitable readout wires (proportional or saturated gas amplification).

different spectral sensitivities [87], or with very thin foils of WLS [91]. Potentially the most promising developments concern scintillators. They are still rather inefficient (only a few percent of the energy loss is converted into visible photons), and reduced saturation of the response to densely ionizing nuclear fragments should improve the energy resolution of hadron calorimeters (see subsection 3.3). The scintillator properties are important for the energy resolution of calorimeters, and need to be carefully investigated and specified when comparing various seemingly equivalent calorimeters.

Interest in high granularity and very compact readouts has recently led to 'double wavelength-shifter' applications [92–95] (Fig. 18). Although the second shifting reduces the number of photons by a further factor of ~ 5, the compression of the light into a very small cross-section light-pipe is attractive for several reasons, such as small insensitive zones and the possibility to use light detectors with small active areas. Such schemes favour the light registration with vacuum photodiodes [56, 70, 96] or silicon photodiodes [59, 93]. These devices—lacking an internal charge amplification mechanism—are operated with low-noise charge-sensitive preamplifiers, and are therefore more stable compared with photomultipliers; furthermore, they are insensitive to the commonly used levels of magnetic fields (vacuum diodes with some restrictions). These light detectors are therefore particularly attractive for the photon calorimeters of storage ring detectors, which most frequently are operated inside magnetic spectrometer fields [49, 56, 59, 60, 70].

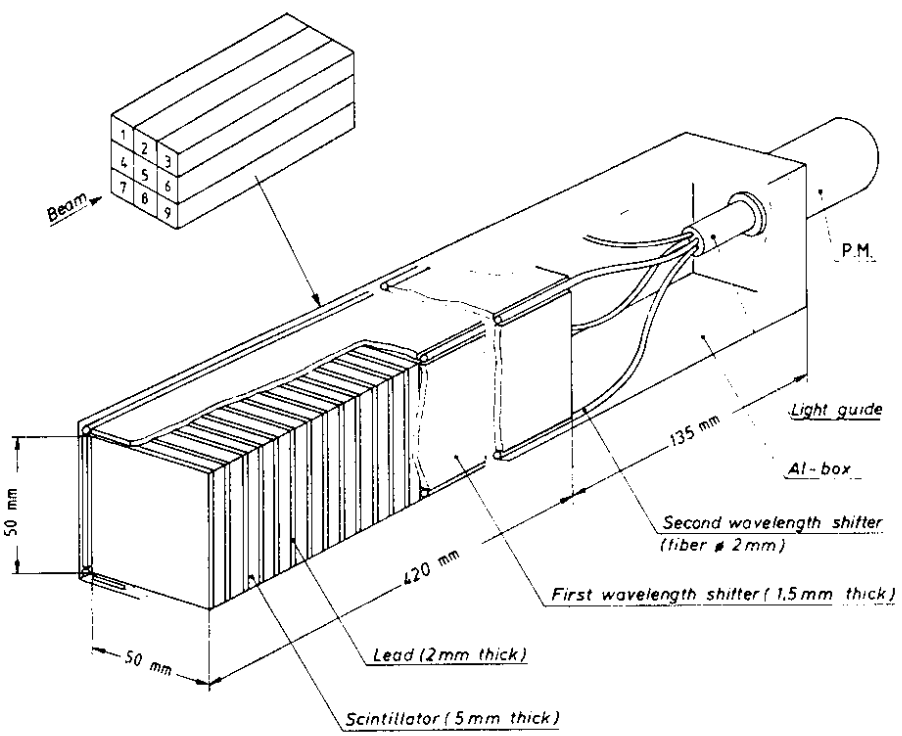

Fig. 18: Schematic view of a 'tower' of a sampling calorimeter array, using double-wavelength shifting techniques for the light measurement. The thin plates of the first WLS cover all four sides of the tower, whereas the second WLS, in the form of a fibre, registers the light emerging from the first shifter and guides it to the photomultiplier [92].

Another line of study concerns the innovative use of scintillators. Very long, narrow, Teflon tubes filled with liquid scintillator have been used for a large photon calorimeter [97]. The Teflon tubes define the spatial granularity of the active element and guide the light through total internal reflection to photomultipliers. A logical refinement consists in using small scintillating fibres [98] embedded in a metal matrix. With this technique a photon detector was constructed with the very short average radiation length of $X_0 = 14.5$ mm and an energy resolution of $\sigma_\gamma/E = 0.11/\sqrt{E}$—the modest man's BGO [99].

In recent years considerable effort was devoted to minimizing two disadvantages of the scintillator readouts; namely, the inherent non-uniformity in the light collection, and the difficulty of energy calibration.

The principal source of non-uniform light collection is not primarily the attenuation of light propagating in thin scintillator sheets, but is usually due to the light collection geometry. The non-uniform response, measured for example by scanning the active surface with a monochromatic electron beam, is at a level of $\pm 5\%$ in finely tuned instruments [32], and one representative example is shown in Fig. 19. Such a level of non-uniform response will of course influence the energy resolution for electrons with $p \geq 10$ GeV/c, if no correction for the impact point is applied. Hadron showers are much less affected, if the geometric extension of the non-uniformities is comparable to or smaller than the shower size. Such problems may be considerably aggravated if the usually sufficiently high transmission of the scintillator is affected, e.g. by radiation damage [32], surface cracking, or for other reasons. Plastic scintillators will show radiation damage after exposure to less than 100 Gy, if in contact with air [100], whilst toluene-based scintillator may sustain approximately 10 times more radiation [101, 102] before its usefulness is severely limited. Closely connected with these problems of light collection is the strategy of relative and absolute energy calibration. For precision applications, it is necessary to expose each calorimeter cell at least once to some kind of particle beam in order to establish an absolute calibration, which subsequently has to be transferred and maintained with some kind of absolutely stable light source. This light source is usually an external reference lamp, whose output is distributed to the calorimeter cells [103]. In some cases, the light produced by internal radioactive sources [32] has served this purpose.

The limitations outlined here become a major concern for applications where very high energy deposits could, in principle, be measured at the one percent accuracy level [50, 95, 104] and correspondingly benefit the quality of the physics data.

Increasingly, therefore, the experimental teams are evaluating alternative solutions, as discussed in the next subsection.

5.2.2. Charge collection readout. The ionization charge produced by the passage of the charged particles of the shower may be collected from solids, liquids, or gases. Solids [105] and liquids can only be used in an ionization chamber mode with no internal amplification. The best known and, to date, the only practical example is based on the use of liquid argon [106]. In specific cases, liquid xenon may be used [107–110]. The use of room-temperature liquids has also been repeatedly advocated [95, 111], but with increasing operating temperature the tolerable level of impurities decreases strongly. If gas is used as the active sampling medium, internal amplification to various degrees is usually exploited: proportional chambers or tubes provide a signal proportional to the

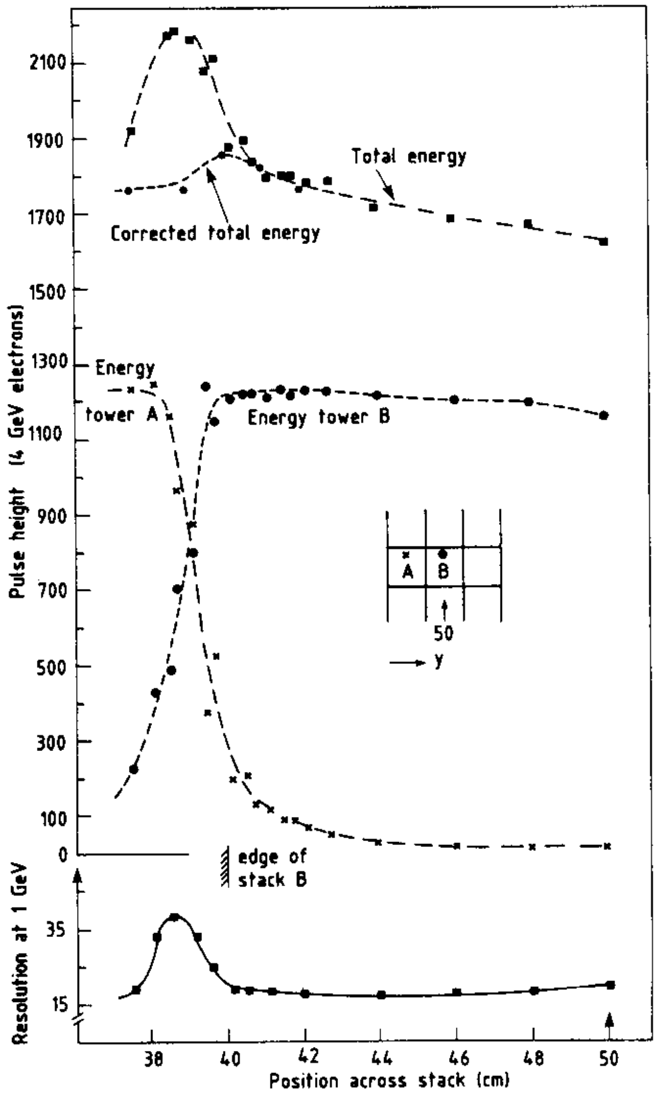

Fig. 19. The worst-case optical non-uniformity obtained by scanning with a 4 GeV/c electron beam under normal incidence across the gap between neighbouring stacks. The approximately 15% non-uniformity can be further reduced with a correction algorithm using the two signals in each tower, A and B (short-dashed curve) [32].

energy loss. At higher gas gain, with devices operating in a controlled streamer or Geiger mode, the measured signal is related to the number of shower particles which traverse the active medium ('digital readout') [112]. The conceptual arrangements are shown in Fig. 20.

The principal advantages common to all these charge collection methods are seen in the ease of segmentation of the readout and the capability to operate in magnetic fields. Some features specific to the various types are:

a) operation in the ionization mode, i.e. liquid-argon calorimeters, provides the best control of systematic effects [44, 113–116];

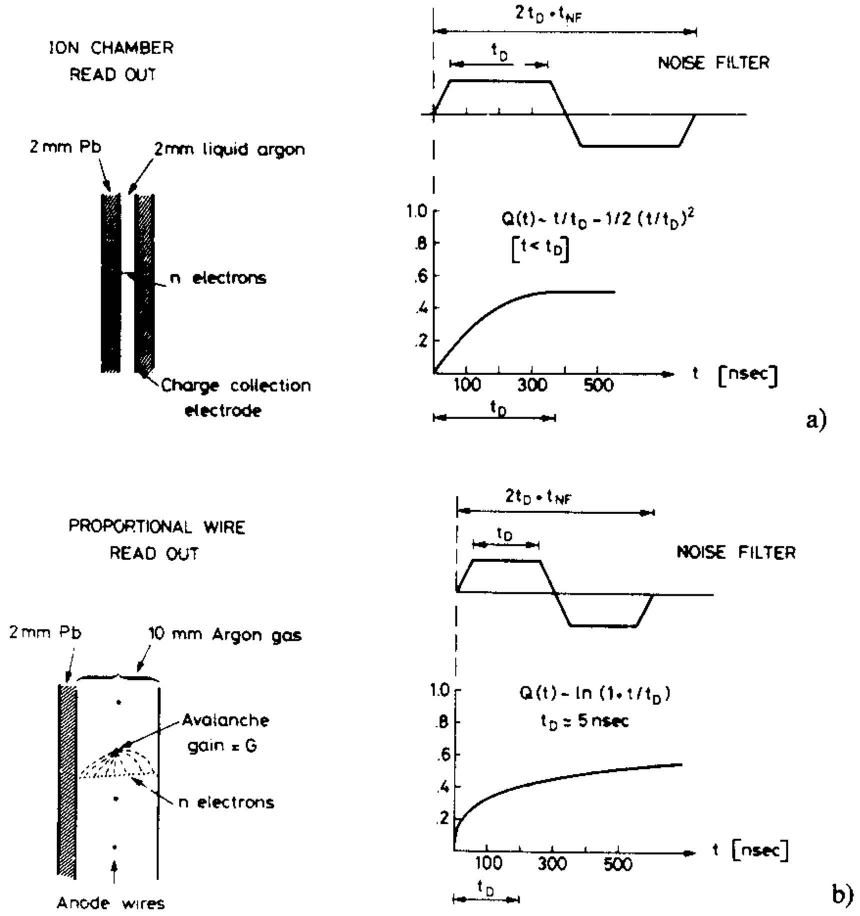

Fig. 20: Charge collection in a single sampling layer for a) a liquid-argon calorimeter with ion chamber readout; b) gas proportional wire readout. The signal charge Q(t) is shown as a function of time, and t_D is the time required for all ionization electrons to be collected. For each case a bipolar noise-filter weighting function is indicated (see text).

b) gas proportional devices offer a wide variety of relatively inexpensive construction methods [117];
c) digital operation, in the Geiger or streamer mode, allows for very simple and cheap signal-processing electronics [112, 118, 119].

The ion chamber technique is the preferred solution whenever optimum performance is at a premium because it excels in the following points, all of which have been realized in practice in devices using liquid argon as the active medium:

- uniformity of response at the fractional percent level;
- ease in fine-grained segmentation with a minimum of insensitive area;
- excellent long-term operating stability (radiation damage absent in liquid argon; response of active medium controllable).

Experimentation at today's fixed-target or storage ring facilities often justifies the use of such high-performance calorimeters, and as a consequence the liquid-argon ion chamber technique has been adopted for several large facilities, both in existence [44, 113–116] or planned [51, 120, 121]. One noteworthy exception is made by the teams preparing the four LEP detectors—they have opted for scintillator or proportional chamber readout solutions.

For many years, several liquid substances have been known, in which electrons may be drifted over large (several centimetres) distances, given adequate electric fields and levels of purity [122]. Generally, it may be said that operation at cryogenic temperatures, $T < 100$ K, eases the purification problem. Liquid-argon calorimeters, for example, may be operated with levels of ~ 1 ppm O_2, but the requirements are already considerably more severe for liquid xenon (~ 10 ppb O_2 tolerable) and develop into a major engineering difficulty for room-temperature liquids [95, 123]. In practical applications one has to weigh the complexity of a cryogenic detector (difficult access to components inside, extra space for the cryostat, increased mechanical engineering problems) against the difficulties arising from impurity control (large multistage purification plant, use of ultra-high vacuum techniques and components in the construction) [123]. It was thought that some of the lighter room-temperature liquids [such as tetramethylsilane (TMS)] might be intrinsically more advantageous for hadron calorimeter readouts, because one expected relatively small saturation for densely ionizing particles (e.g. recoil protons) [124]. Recent measurements [95, 125] however, have indicated that in practical electric drift fields such an advantage may not exist.

The very low cost of sufficiently pure liquid argon and the relative ease of maintaining it in operating conditions suggest its use in large-mass detectors for neutrino-scattering or proton-decay experiments [77–79, 126]. As with all rare-event detectors, the possibility of very large drifts of the ionization [time projection chamber (TPC)] have been studied with the aim of reducing the number of electronic channels to an 'acceptable' level [76, 77].

A recent extension of the ion chamber techniques to the use of solid dielectrics has met with considerable success [127], the signal being measured with Si surface barrier detectors in sampling calorimeter detectors. This scheme combines the advantages of a room-temperature ion chamber readout, with the attractive feature that these Si detectors are usually extremely thin, less than 500 μm, permitting the realization of detectors with $X_0 \leq 4$ mm, and hence offering the ultimate localization of showers.

For ion chambers and proportional wire readout, the measured signal typically amounts to a few picocoulombs of charge per GeV of shower energy. Since sampling calorimeters are inherently devices having a large capacitance, the optimum charge measurement requires careful consideration of the relationship between signal, noise, resolving time, and detector size. A detailed noise analysis gives [128]

$$ENC_{opt} = k \times 10^6 (C_D/t_{NF})^{1/2},$$

the 'equivalent noise charge' ENC being the input signal level which gives the same output as the electronic noise. The parameter k is proportional to the r.m.s. thermal noise of the input field-effect transistor; for practical detector arrangements a value of $k \simeq 5$ is realized. [C_D is the detector capacitance (in μF), and t_{NF} is the noise filter-time (in ns)]. This relation determines the fundamental lower limit to the noise, which is achieved with optimal capacitance matching between the detector and amplifier. The noise figure grows with increasing detector capacitance, but can be reduced at the expense of augmenting the resolving time.

Charge collection in gases, usually followed by some degree of internal amplification, forms the basis of another important category of calorimeter readouts [117]. The method lends itself naturally to highly segmented construction, of particular value for the topological analysis of the energy deposit (e.g. γ/hadron discrimination, muon identification). The technique has profited from the diversified developments in gaseous position detectors [129] over the last fifteen years: the versatility of arranging readout anode wires combined with the ease of gain control have produced a great variety of different solutions tailored to the specific requirements of an experiment.

With these types of detectors, spatial segmentation and localization can be easily implemented. This may be achieved in a projective geometry using strips, or in a 'tower' arrangement, e.g. by measuring the signal charge induced on a pattern of cathode pads [130, 131]. The tower arrangement is mandatory for reducing ambiguities and confusion in multiparticle events.

Another technique, currently being pursued, aims at achieving a very high degree of spatial segmentation, and uses a TPC method, the so-called 'drift-collection' calorimeter [132]. The ionization produced by the charged particles of a cascade is drifted over very long distances and collected on a relatively small number of proportional wire planes, equipped with a two-dimensional readout, while the third shower coordinate is determined by a drift-time measurement. The conceptual configuration is shown in Fig. 21. An example of the pictorial quality of shower reconstruction expected with this technique is given in Fig. 22.

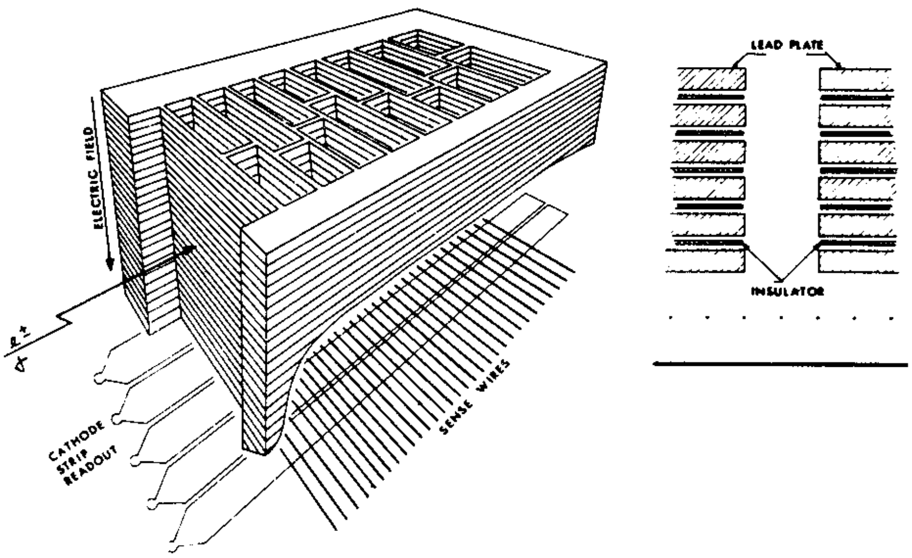

Fig. 21: Geometrical arrangement for the high-density drift calorimeter. Cavities between absorber plates allow the drifting of ionization electrons over long distances on to MWPC-type detectors. Very high spatial granularity can be achieved at the cost of mechanical complexity and rate capability. A very uniform magnetic guidance field parallel to the drift direction is usually required [132].

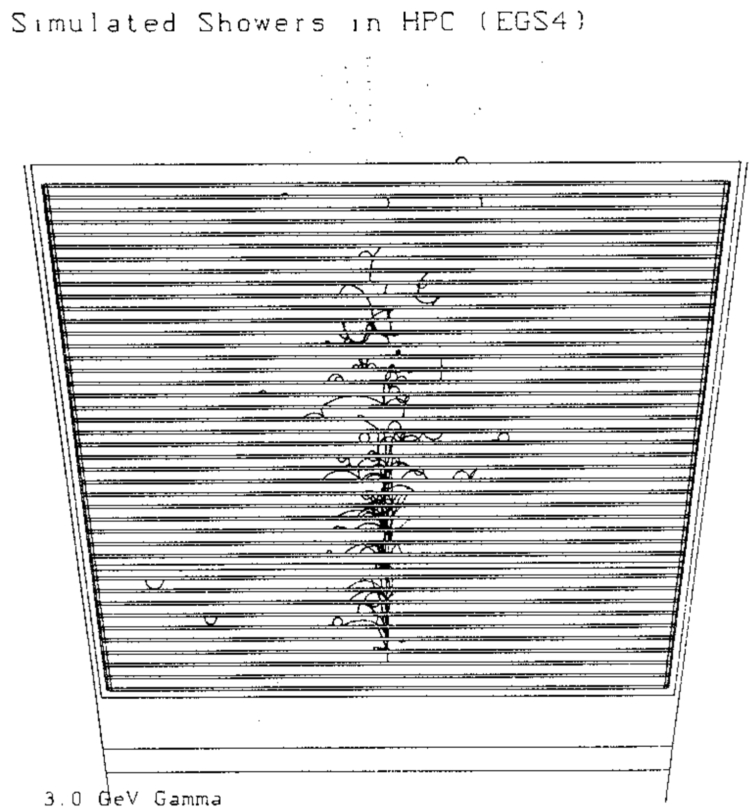

Fig. 22: Simulation of an electromagnetic shower in the calorimeter of the LEP DELPHI collaboration using EGS IV. The bubble-chamber-like pictorial quality of the information allows the individual shower particles to be distinguished. (Courtesy of H. Burmeister, CERN.)

Gas sampling calorimetry in a digital mode (using Geiger, streamer, or flash-tube techniques) is a means of simplifying the signal processing circuitry, and offers an expedient method for achieving a high degree of segmentation. Flash chambers consist of an array of tubular cells filled with a mixture of about 96% neon + 4% helium; a pulsed high-voltage is applied across each cell after an external event trigger. In the presence of ionization charge, a signal-producing plasma discharge propagates over the full length of the cell. In one such array for a large neutrino experiment at Fermilab, 608 flash-chamber planes with a total of some 400,000 cells are sandwiched between absorber layers of sand and steel shot [24]. The pattern of struck cells in each plane is read out by sensing induced signals on a pair of magnetostrictive delay lines. Wire readout planes may also be operated in the 'streamer mode', where the charge gain is controlled to cover only a segment around the particle impact point [133, 134]. Common to these saturated gas-gain readout schemes are the following properties:

- the energy resolution is in principle better than in a proportional gain system, because Landau fluctuations are reduced or suppressed;
- the mechanical tolerances of the readout system are less stringent than for proportional systems;

- these readouts are inherently non-linear. One charged particle causes an insensitive region along the struck wire, which prevents other nearby tracks from being registered. Typically, non-linearities become measurable above ~ 10 GeV.

Usually, care is taken to limit the geometrical extension of the discharge region, e.g. with various mechanical discontinuities (beads, nylon wires, etc.). A calorimeter operated in this mode gave an energy resolution of $\sigma \simeq 14\%/\sqrt{E}$ for electron energies up to 5 GeV [135]. This is better than is normally achieved for gas sampling calorimeters, reflecting the absence of Landau and path-length fluctuations. At higher energies the calorimeter showed saturation effects due to the increasing probability of multiple hits over the geometrical extension of the discharge region.

The *rate capability* of calorimeters is an important parameter for high-rate fixed-target experiments or the planned hadron colliders (Table 8) [136]. Several different time constants characterize the readout:

1) 'occupation' time specifies the length of time during which the physical signal produced by the particle is present in the detector (pulse length);
2) 'integration' time corresponds to the externally (e.g. electronically) chosen time defining the bandwidth of the signal processing system;
3) 'time resolution' specifies the precision with which the impact time of a particle may be determined.

For scintillator-based methods the signal duration is typically about 20–50 ns but, with special care, signals of about 10 ns length have been achieved [94].

For liquid-argon devices, the charge-collection time is ~ 200 ns/mm gap; it may be reduced by a factor of 2 by adding ~ 1% of methane. Sometimes it is acceptable not to integrate over the full signal length, entailing a reduction in the signal-to-noise ratio. For liquid-argon devices, the noise is proportional to $(\tau_{\mathrm{integ}})^{-1/2}$ and the signal is almost proportional to $(\tau_{\mathrm{integ}})^{1/2}$, if $\tau_{\mathrm{integ}} < \tau_{\mathrm{tot.\ coll.}}$. A very short integration time is sometimes chosen ('clipping' of a signal) to enable very fast trigger decisions; only if the event information is of interest is the signal processed with a longer integration time, in order to obtain an optimum signal-to-noise ratio.

The time resolution achievable with calorimeters may help to associate the calorimeter information with different events, separated by a time interval much shorter than the integration time. For scintillator and liquid-argon calorimeters, time resolutions of 2–3 ns have been measured for few-GeV energy deposits [44, 137].

The ultimate rate limitation is, however, determined by the physics to be studied with a calorimeter. In collisions involving hadrons in the initial state, reactions which occur with very different cross-sections may be characterized by very different event topologies. A typical example is the production of several high-p_T jets in a pp collision, the cross-section of which is very small in comparison with the total inelastic cross-section. In such a case, several events may be recorded within the occupation time of the detector without serious effects (Fig. 23). This figure suggests that calorimeters may still be very useful even if, during the occupation time of an interesting event, several other events produce energy deposits and are recorded in the detector [32, 39, 138].

Table 8: Temporal Response of Readout Systems

Calorimeter system	Occupation time (ns)	Pulse width (integration) (ns)	Timing resolution σ (ns)	Radiation resistance
Metal/scintillator with WLS readout	50	50	2.5 for few-GeV deposit; better at higher energy, if not limited by PM	Depends on scintillator, dose rate, environment; $> 10^3$ Gy appear achievable [102].
^{238}U/scintillator with fast WLS readout	~ 100	100	2.5	As above
Metal/fast scintillator with fast WLS readout	$\leqslant 20$	$\leqslant 20$	< 2 (?)	
Metal/proportional or saturated gas-gain readout	50–100	100–200 bipolar shaping	$\leqslant 10$	Adequate for chamber; lifetime of on-detector electronics may be a limitation; readout elements need to be shielded from U radioactivity.
^{238}U/proportional or saturated gas-gain readout	$\geqslant 100$	$\geqslant 200$ bipolar shaping	$\leqslant 10$	
Metal/LAr ion chamber	~ 200 per 1 mm gap	$2\lambda = 400$ bipolar shaping	~ 2 for few-GeV deposit	Lifetime of on-detector electronics may be a limitation
Metal/LAr–CH_4 ion chamber	~ 100 per 1mm gap	$2\lambda \leq 200$	$\lesssim 2$ for few-GeV deposit	NB: shorter pulse width (2λ) possible the expense of signal/noise $\simeq \lambda^{\alpha}$, at $\alpha \sim 1$.

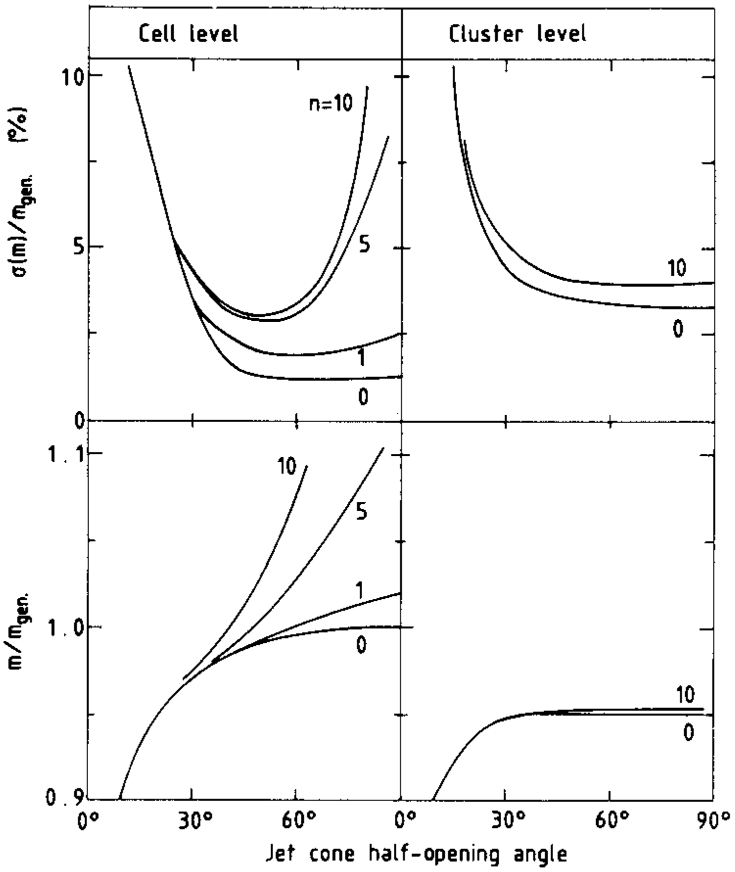

Fig. 23: Two-jet mass resolution (upper part) and reconstructed mass value (lower part) for a 1 TeV system at the cell and at the cluster level as a function of the opening angle between the jets, and the number n of additional accidental minimum-bias events [39] (see Fig. 14 for definition of cell and cluster level).

5.2.3. Bolometric Readout. Repeatedly, particles have been detected through the temperature rise in a calorimeter, caused by the absorption of the particles. Such experiments contributed decisively to our understanding of radioactivity and to the concept of the neutrino [139]. Already 50 years ago it was recognized that owing to the large reduction in heat capacity of many materials at cryogenic temperatures, very sensitive instruments were permitted [140]. More recently, interest has refocused on cryogenic calorimetry, operated in the temperature range of 1 mK to ~ 1 K. Such detectors [141–143] are considered as possible particle detectors offering an energy resolution of ≤ 10 eV and having a time response in the 100 μsec to 1 msec range. Possible experiments include the search for double-beta decay or the measurement of the end point of tritium beta decay. More ambitiously, multiton silicon detectors operated at mK temperatures are considered as a solar neutrino observatory to measure the spectrum of solar neutrinos and to probe for neutrino mass differences at the 10^{-6} eV level. Cryogenic calorimetry promises far more precise energy measurements than any of the other 'standard' techniques and allows us to contemplate some of the most challenging and fundamental experiments in particle physics.

6. SYSTEM ASPECTS OF CALORIMETERS

6.1 General Scaling Laws of the Calorimeter Dimensions

A number of parameters which may be external to the calorimeter design, e.g. the dimensions of a charged-particle spectrometer, may ultimately determine the size of a calorimeter.

If, however, global optimization of an experiment is attempted, one should aim for the most compact calorimeter layout that may lead to the achievement of the physics goals of the detector.

The distance D of a calorimeter from the interaction vertex, and hence its necessary size, is determined by the achievable useful segmentation and the characteristic angular dimension θ required to be resolved in the measurement. The useful segmentation d is determined by the shower dimensions, approximately $d \sim 2\varrho_M$ for electromagnetic detectors and $d \sim \lambda$ for hadronic ones. The characteristic angular dimension θ may be the minimum angular separation of the photons from π^0 decay, or the typical angle between the energetic particles in a hadron jet.

For correctly designed detector systems, the calorimeter dimensions are determined by the angular topology and size of the showers to be measured. The minimum detector distance is then $D \geq d/\mathrm{tg}\,\theta$, and the required calorimeter volume V is found to be

$$V \propto D^2 \times L \text{ (depth of calorimeter required for total absorption)}$$

whence

$$V \propto \varrho_M^2 \times X_0 \text{ for e.m. detectors,}$$

and

$$V \propto \lambda^2 \times \lambda \text{ for hadronic detectors.}$$

The third-power dependence of the calorimeter volume on shower dimensions implies that it may be economically advantageous to select very compact calorimeter designs, even if the price per unit volume is very high. Table 9 explains why sometimes only the most expensive materials (per cm^3) can be afforded.

6.2. Calorimeter Systems for Physics Applications

6.2.1 Neutrino physics and nucleon stability. Detectors for these studies share some common features: the event rate is low and is proportional to the total instrumented mass; the physics requires a fine-grained readout system, which permits detailed three-dimensional pattern reconstruction. Bubble chambers have therefore been used extensively but are limited by the long analysis time per event. The present generation of neutrino detectors makes extensive use of wire-chamber techniques to approach the intrinsic spatial and angular resolution of calorimeters. New 'visual' electronic techniques are being developed for proton decay experiments, for which very massive detectors with a high density of signal channels are required.

A neutrino detector, even when exposed to present-day intense neutrino beams, must have a very large mass (typically hundreds of tons), and its volume must be

Table 9: Characteristic Dimensions and Price Comparisons for e.m. Calorimeters

Material / Quantity	NaI	BGO	U/Si sampling calorimeter
X_0 (mm)	26	11	4
ϱ_M (mm)	44	23	11
Reference volume (cm^3) for 95% containment of ~ 5 GeV electrons	1600	180	15
Approx. price/Ref. vol. (arbitrary units)	1	1	0.1

uniformly sensitive to the signature that an interaction has occurred and to the characteristics of the reaction products. These requirements explain the modular construction typical of modern electronic neutrino detectors. The general form of the interaction is $\nu_{(\mu,e)}$ + nucleon = $\ell_{(\mu,e)}$ + X, where ℓ is a charged lepton (charged-current interaction) or a neutrino (neutral-current interaction), and X represents the hadronic system. The signature for a neutrino interaction is the sudden appearance, in the detector, of a large amount of energy in a few absorber layers. If the scattered lepton is a muon, it leaves in each layer the characteristic signal of a single minimum-ionizing particle. In some detectors the absorber layers are magnetized iron, which makes possible a determination of the muon momentum from the curvature of its trajectory. For a detailed study of neutral-current interactions, a very fine grained subdivision of the calorimeter system is required for measuring the energy and direction of the hadronic system X and for reconstructing the 'missing' transverse momentum of the final-state neutrino.

Clearly the scope and sensitivity of neutrino experiments would be much improved if even the most massive detectors could resolve final state particles with the reliability and precision typical of a bubble chamber. With this goal in mind, some schemes are currently being investigated that use drift chamber methods with large volumes of liquid argon [79], which provides a visual quality characteristic of homogeneously sensitive detectors. In another case [144] a cylindrical detector, 3.5 m in diameter and 35 m long, is foreseen, containing about 100 tons of argon gas at 150 atm pressure, with ionization electrons collected on planes of anode wires. The idea has also been advanced [145] of using compressed mixtures of more common gases (air or freon), large liquid-argon TPCs [78], or room-temperature liquid hydrocarbons [146] to detect the ions that migrate away from charged-particle tracks (positive and/or negative ions produced by electron attachment).

Detectors to search for the decay of nucleons are also characterized by a very large instrumented mass, varying from a hundred to several thousand tons. Current theoretical estimates place the proton lifetime at around $\tau_p \simeq 3 \times 10^{29 \pm 1.5}$ y compared with present experimental limits [147] of $\tau_p \geq 10^{32}$, reached by detectors of at least 1000 tons mass, or approximately $> 10^{33}$ nucleons. These detectors have to be instrumented to search sensitively for some of the expected decay modes such as $p \rightarrow e^+ + h^0$, where h^0 is a neutral meson (π^0, η, ϱ^0, ω^0). The signature of such a decay is clear, provided a detector is sufficiently subdivided to recognize the back-to-back decay into a lepton and a hadron with the relatively low energy deposit of about 1 GeV. The sensitivity is limited by the flux of muons and neutrinos originating from atmospheric showers. Only muons can be shielded by placing the experiments deep underground in mine shafts or in road tunnels beneath high mountains. The ν_μ-induced rate simulating nucleon decay is estimated at $\sim 10^{-2}$ events per ton per year if energy deposition alone is measured. If complete event reconstruction is possible, an experimental limit of $\tau \geq 10^{33}$ y may be reached [147].

The most massive calorimetric detectors to date have been conceived to explore the very high energy cosmic-ray spectrum. The detector volumes needed are so large that only the sea water [148] and air [149] are available in sufficiently large quantities. The interaction provoked by cosmic-ray particles is detected through the Cherenkov radiation emitted in the ensuing particle cascade in the case of the deep underwater array. In the case of the atmospheric detector it is the light from the excited N_2 molecules which is detected and measured with great ingenuity. The 'air calorimeter' represents the largest ($V \simeq 10^3$ km^3) and most massive ($W \sim 10^9$ tons) calorimeter conceived to date; already it has produced evidence about the cosmic-ray flux at $E > 10^{20}$ eV.

6.2.2. Calorimeter facilities for storage rings. At hadron machines the studies focus on reactions that are characterized by a large transverse energy (E_T) flow, as a signal for an inelastic interaction between the nucleon constituents. The signature appears in many different characteristic event structures and may therefore be efficiently selected with hadron calorimeters : examples are single high-p_T particles, 'jets' of particles, or events exhibiting large E_T, irrespective of their detailed structure. Topical applications include invariant mass studies of multijet events, often in conjunction with electrons, muons, or neutrinos (missing E_T). The power of this approach has been demonstrated by the results obtained in recent years at the CERN $p\bar{p}$ Collider [52], which in turn have led the UA1 and UA2 collaborations to proceed with major upgradings or replacements of their calorimeter detectors [95, 150]. This central role of calorimetry in exploratory hadronic physics programmes [39, 151, 152] is also recognized in the planning for the second detector facility for the FNAL Tevatron. The group is planning a 400 ton uranium/liquid-argon hadron calorimeter, which is expected to be the most advanced calorimeter facility in use during the coming years [51].

At electron–positron colliders, electromagnetic detectors are frequently used to measure the dominant fraction of neutral particles, the π^0's. They are also the ideal tool for detecting electrons, which may signal decays of particles with one or more heavy (c, b, ...) quarks. Unique investigations of cc and bb quark spectroscopy were accomplished with high-resolution NaI shower detectors [153].

For the physics programmes at LEP [154–156] and at the SLAC Linear Collider [120, 157] extensive use of hadron calorimetry will be made. At e^+e^- machines the event topology—production of particles at relatively large angles, with a total energy equal to the centre-of-mass (c.m.) collision energy, favours the experimental technique of total energy measurement. For future e^+e^- physics this method will be important because

- the fraction of neutron and K_L^0 production, measurable only with hadronic calorimeters, increases with energy [158];

- a large and most interesting fraction of events will contain neutrinos in the final state; missing energy and momentum analysis provides the sole handle for such reactions;

- a considerable fraction of events will show good momentum balance but large missing energy—these may be two-photon events or, above the Z^0 pole, events on the radiative tail; total energy will provide the cleanest signature;

- hadronic calorimeters will be the most powerful tool for measuring the reaction $e^+e^- \rightarrow W^+W^-$, either in channels where each W decays hadronically (a total of four jets) or through leptonic decay channels;

- most importantly, a measurement of energy topology is a powerful way of unravelling very rare and unexpected physics phenomena [159].

The technically most difficult requirements for the calorimetry will be imposed by the physics programme at HERA (DESY, Hamburg) [160]. Owing to the very asymmetric energy of the beams (800 GeV protons on 30 GeV electrons), the jets of particles fragmenting from the scattered quarks will have to be measured with the greatest possible energy and *angular* precision in a geometry similar to that of a fixed-target experiment. This implies that the detectors will have a very asymmetrical arrangement, a very large dynamic range, and very high granularity. Innovative developments [93, 127] signal the HERA groups' anticipation of this challenge.

At e^+e^- machines the performance with respect to the energy and space resolution of a well-designed calorimeter is matched to the physics programme foreseen at LEP and at the SLC. Consider, as an example, a 100 GeV multijet event of which the total energy can be measured with an accuracy of $\sigma \simeq$ 3–5 GeV and the total momentum balance checked at a level of $\sigma = 3$ GeV/c. These are intrinsic performance figures, disregarding possible instrumental effects (see Section 3). At hadron colliders, however, a further serious difficulty arises from the convolution of the energy response function with the steeply falling p_T distribution of hadronically produced secondaries [161–164]. As a consequence, the measured energy deposit E' in the detector will originate predominantly from incident particles with energy $E < E'$; count rates and trigger rates are higher than the true physics rates. The result can be devastating for detectors with poor energy resolution or a non-Gaussian response function ('tails' in energy resolution), introducing large errors in the deconvolution. The problem is compounded if the calorimeter response is different for charged and neutral pions (see Section 3): without adequate precautions, these detectors would preferentially select π^0's, making the use of calorimeters marginal for general trigger applications.

The trigger capability is a unique and perhaps the most important requirement of hadron calorimeters employed at hadron machines. For satisfactory operation, one needs uniform response irrespective of event topology and particle composition; good energy resolution at the trigger level to minimize effects of the response function; and adequate granularity for the selection of specific event topologies. For high selectivity, rather complex analogue computations are required, as may be seen from the examples in Table 10 [165]. A tabular summary on calorimeter facilities may be found in Ref. [3].

Table 10: Triggering with Hadron Calorimeters

Experiment	Trigger
Single-particle inclusive distribution; correlations	Localized energy deposit in spatial coincidence with matching track; several thresholds used concurrently.
Jet studies	Extended (~ 1 sr) energy deposit; several thresholds and multiplicities.
Inclusive leptons, multileptons	Electromagnetic deposit in spatial coincidence with matching track; several thresholds and multiplicities.
Heavy flavour jets; correlations	Various combinations of above triggers.

6.3 Monte Carlo Simulations

The development of calorimeters from crudely instrumented hadron absorbers to finely tuned precision instruments owes much to the development of a number of simulation codes. The relatively simple physics governing the electromagnetic showers has facilitated their Monte Carlo simulation. Today, one program has emerged as the world-wide standard for simulating e.m. calorimeters [166]. It has progressed through several improvement stages up to the currently used version, EGS IV, which allows one to follow the shower history, tracking electron pairs down to zero kinetic energy and photons down to ~ 100 keV. It has successfully passed many very detailed tests, including the perhaps ultimate one, that of simulating absolutely the response of electrons relative to muons [167].

The physics and consequently its simulation are considerably more complex for hadronic showers. Over the last decade several programs have been developed, the aim of which is to simulate fairly accurately the detailed particle production of a hadronic cascade [25, 168, 169]. As an example, the flow chart of one of the most detailed simulations is shown in Fig. 24. The attentive reader will no doubt realize that even the most faithful physics simulation of the hadronic process will not guarantee unconditional success. Already the uncertainties associated with the sampling medium (relative response to minimum and heavily ionizing particles) and the complexities of the nuclear interactions are too large to make an *ab initio* calculation possible at present. These programs therefore do require careful tuning against many different measurements, before they become a reliable guide for designing new facilities. The results of a sample calculation are shown in Fig. 25 and give an impression of the power of this code. The status of these shower calculations has recently been extensively discussed [170].

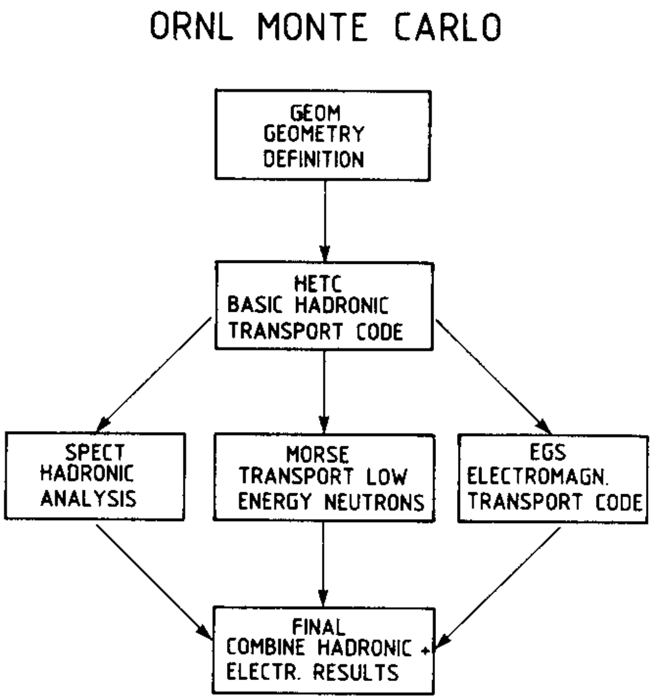

Fig. 24: Flow chart of the hadronic cascade Monte Carlo [T.A. Gabriel et al., Nucl. Instrum. Methods 195:461 (1982)].

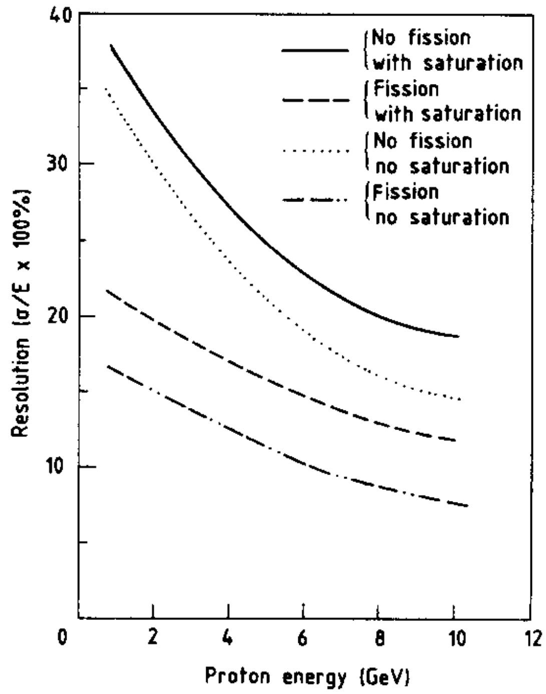

Fig. 25: Results of a 'Gedanken-experiment' using HETC to study the importance of the fission contribution and its manifestation is different readouts, with and without saturation [T. Gabriel et al., Nucl. Instrum. Methods. 164:609 (1979)].

7. OUTLOOK

The use of calorimetric methods in high-energy physics began with rather specialized applications, which capitalized on some unique features not attainable with other techniques: electromagnetic shower detectors for electron and photon measurements; neutrino detectors; and muon identifiers.

The evolution towards a more general detection technique—similar in scope to magnetic momentum analysis—had to wait for extensive instrumental developments driven by strong physics motivations. The application of this technique to the hadron storage rings (which were inaugurated in the early 1970's) was therefore delayed, but it has shaped the detectors for the CERN $p\bar{p}$ Collider and has proved to be of major importance for the detector facilities currently in preparation. At the same time, physics studies have evolved along lines where measurements based on 'classic' magnetic momentum analysis are supplemented or replaced by analyses which are based on precise global measurements of event structure, frequently requiring extraordinary trigger selectivity, and which are much more suitable for calorimetric detection. During the next decade, experiments will rely increasingly on these more global studies, with properties averaged over groups of particles and with the distinction between individual particles blurred, unless they carry some very specific information. This role of calorimetry in both present and planned physics programmes is summarized in Table 11; the impact of instrumental advances and technology is outlined in Table 12.

Table 11: Future Role of Absorptive Spectroscopy

Source of particles	Physics emphasis	Calorimeter properties	Technical implications
pp ($p\bar{p}$) collider	Rare processes: high-p_T lepton, photon production; manifestations of heavy quarks $W^{\pm}$, Z^0, ...	$\sim 4\pi$ coverage with e.m. and hadronic detection; high trigger selectivity	Approach intrinsic resolution in multicell device; control of inhomogeneities, stability
e^+e^- collider	Complex high-multiplicity final states (multijets, electrons in jet, neutrinos)	Precision measurements of total visible energy and momentum	Very high granularity; particle identification
ep colliders (secondary beams, $p \geq 1$ TeV/c)	High-multiplicity final states; strong emphasis on global features	Calorimeter becomes primary spectrometer element	High granularity, high rate operation
Penetrating cosmic radiation; proton decay	Detailed final-state analysis of events with extremely low rate	Potentially largest detector systems ($\geq$ 10,000 tons) with fine-grain readout	Ultra-low-cost instrumentation

Table 12: Interdependence of Detector Physics and Technologies for Calorimeters

Principles	Electronics	Mode of operation
Improved understanding of limitation to energy resolution in hadron calorimeters	Gain stability at ~ 1% gain monitoring at 0.1% of ~ 10^5 analogue channels	
Calorimeters replace magnetic spectrometers at high energies	Operational systems of ~ 10^5 light- or charge-measuring channels	Very high spatial resolution for electromagnetic and hadronic showers
Particle identification through energy deposit pattern (μ, e, γ, π^0, n, $\bar{p}$, K^0_L, ν)	Cheap, fast ADC for high-level fast trigger decisions	Helps or allows pattern recognition of very complex events (jets, ...)

Despite recent conceptual and technical progress, a number of questions deserve further attention:

1) What is the precise energy dependence of hadronic energy resolution?
2) What improvement in energy, position, and angular resolution could be obtained with complete information on the individual shower distributions? With such information, could we minimize the effect of increased longitudinal leakage on the energy resolution?
3) What contributes to the measured energy resolution $\sigma(E) \simeq 0.2 \times E^{-1/2}$ of a fission-compensated hadron calorimeter?
4) Is there a cure for the low-energy non-linearities?
5) Can we understand hadronic sampling fluctuations to the same degree as we understand electromagnetic ones?
6) Can particle identification and separation be improved if more detailed shower information is available?
7) Are there any advantages in mixing different absorber materials, or in changing the sampling step inside a calorimeter?
8) Can we tailor the signal response of the readout to improve the calorimeter response?

The very diverse applications of calorimetric techniques will ensure continued study of these and the many technical questions connected with the signal processing of calorimeter information. There can never be a unique solution, but there should always be a search for the most suitable method. We hope that the information provided in this review will be useful for attaining this goal.

ACKNOWLEDGEMENTS

I wish to express my appreciation to Professor T. Ferbel who, as director of the 'Advanced Institute', has developed a School, which by its size, its students, its style, and its 'ambiance' appears optimally conducive to the pursuance of a variety of very topical themes.

R. Wigmans helped me considerably with a critical reading of these notes. C. Comby, L. Karen-Alun, M. Mazerand, M.-S. Vascotto, and K. Wakley efficiently and cheerfully converted my manuscript into printable form.

REFERENCES

[1] V.S. Murzin, Progress in elementary particle and cosmic-ray physics, J.G. Wilson and I.A. Wouthuysen, eds., North Holland Publ. Co., Amsterdam (1967), Vol. 9, p. 247.
[2] M. Atac, ed., Proc. Calorimeter Workshop, Batavia, 1975, FNAL, Batavia, Ill. (1975).
[3] C.W. Fabjan and T. Ludlam, Ann. Rev. Nucl. Part. Sci. 32:335 (1982).
[4] U. Amaldi, Phys. Scripta 23:409 (1981).
[5] S. Iwata, Nagoya University report DPNU-3-79 (1979).
[6] H. Messel and D.F. Crawford, Electron-photon shower distribution: Function tables for lead, copper and air absorbers, Pergamon Press, London (1970).
[7] Y.S. Tsai, Rev. Mod. Phys. 46:815 (1974).
[8] B. Rossi, High-energy particles, Prentice Hall, New York (1964).
[9] E. Longo and I. Sestili, Nucl. Instrum. Methods 128:283 (1975).
[10] H.H. Nagel, Z. Phys. 186:319 (1965).
[11] D. F. Crawford and H. Messel, Phys. Rev. 128:2352 (1962).
[12] Yu.D. Prokoshkin, Proc. Second ICFA Workshop on Possibilities and Limitations of Accelerators and Detectors, Les Diablerets, 1979, U. Amaldi, ed., CERN, Geneva (1980), p. 405.
[13] E.B. Hughes et al., IEEE Trans. Nucl. Sci. NS-19: 126 (1972).
[14] H.G. Fischer, Nucl. Instrum. Methods 156:81 (1978).
[15] R.W. Sternheimer et al., Phys. Rev. B3:3681 (1971).
[16] K. Pinkau, Phys. Rev. B139:1548 (1965).
[17] T. Yuda, Nucl. Instrum. Methods 73:301 (1969).
[18] C.J. Crannel, Phys. Rev. 182:1435 (1969).
[19] T. Kondo et al., A simulation of electromagnetic showers in iron-lead and uranium-liquid argon calorimeters using the EGS, and its implication for e/h ratios in hadron calorimetry, contributed paper to the Summer Study on the Design and Utilization of the Superconducting Super Collider, Snowmass, Colo. (1984).
[20] G.A. Akopdjanov et al., Nucl. Instrum. Methods 146:441 (1977).
S.R. Amendolia et al., Pisa 80-4.
R. Rameika et al., Measurement of electromagnetic shower position and size with a saturated avalanche tube hodoscope and a fine grained scintillator hodoscope, to be published in Nucl. Instrum. Methods.
[21] T. Kondo and K. Niwa, Electromagnetic shower size and containment at high energies, contributed paper to the Summer Study on the Design and Utilization of the Superconducting Super Collider, Snowmass, Colo. (1984).
[22] E. Gabathuler et al., Nucl. Instrum. Methods 157:47 (1978).
[23] A.N. Diddens et al., Nucl. Instrum. Methods 178:27 (1980).
[24] D. Bogert et al., IEEE Trans. Nucl. NS-29:336 (1982).
[25] J. Ranft, Particle Accelerators 3:129 (1972);
A. Baroncelli, Nucl. Instrum. Methods 118:445 (1974);
T.A. Gabriel et al., Nucl. Instrum. Methods 134:271 (1976).
[26] R. Bock et al., Nucl. Instrum. Methods 186:533 (1981).
[27] C.W. Fabjan and W.J. Willis, Proc. Calorimeter Workshop, Batavia, 1975, M. Atac ed., FNAL, Batavia, Ill. (1975), p. 1.
C.W. Fabjan et al., Phys. Lett. 60B:105 (1975).
[28] O. Botner, Phys. Scripta 23:555 (1981).
[29] A. Benvenuti et al., Nucl. Instrum. Methods 125:447 (1975).

[30] M.J. Corden et al., Phys. Scripta 25:5 (1982).
[31] A. Beer et al., Nucl. Instrum. Methods 224:360 (1984).
[32] T. Akesson et al., Properties of a fine sampling uranium-copper scintillator hadron calorimeter, submitted to Nucl. Instrum. Methods (1985).
[33] T. Gabriel and W. Selove, private communication.
[34] U. Amaldi and G. Matthiae, private communications.
[35] H. Abramowicz et al., Nucl. Instrum. Methods 180:429 (1981). See also, for earlier work, J.P. Rishan, SLAC 216 (1979).
[36] Results similar to those given in [35] were recently obtained by the WA78 Collaboration at the CERN SPS (P. Pistilli, private communication).
[37] C.W. Fabjan et al., Nucl. Instrum. Methods 141:61 (1977).
[38] W.J. Willis, Invited talk given at the Discussion Meeting on HERA Experiments, Genoa (1984).
[39] T. Akesson et al., Proc. ECFA-CERN Workshop on a Large Hadron Collider in the LEP Tunnel, Lausanne and Geneva, M. Jacob, ed., CERN 84-10 (1984).
[40] F. Binon et al., Nucl. Instrum. Methods 188:507 (1981).
[41] A.V. Barns et al., Phys. Rev. Lett. 37:76 (1970).
See also T. Ferbel, Understanding the fundamental constituents of matter, A. Zichichi, ed., Plenum Press, New York, NY (1978).
[42] J.A. Appel et al., Nucl. Instrum. Methods 127:495 (1975).
D. Hitlin et al., Nucl. Instrum. Methods 137:225 (1976).
R. Engelmann et al., Nucl. Instrum. Methods 216:45 (1983)
U. Micke et al., Nucl. Instrum. Methods 221: 495 (1984).
[43] M. Basile et al., A limited-streamer tube electron detector with high rejection power against pions, to be published in Nucl. Instrum. Methods (1985).
[44] J. Cobb et al., Nucl. Instrum. Methods 158:93 (1979).
[45] J. Ledermann et al., Nucl. Instrum. Methods 129:65 (1975).
[46] L. Baum et al., Proc. Calorimeter Workshop, Batavia, 1975, M. Atac, ed., FNAL, Batavia, Ill. (1975), p. 295.
A. Grant, Nucl. Instrum. Methods 131:167 (1975).
M. Holder et al., Nucl. Instrum. Methods 151:69 (1978).
[47] A. Bodek et al., Phys. Lett. 113B:77 (1982).
[48] K. Eggert et al., Nucl. Instrum. Methods 176 (1980) 217.
[49] Technical Proposal of the L3 Collaboration, CERN/LEPC/83-5 (1983).
[50] H. Gordon et al. (HELIOS Collaboration), Lepton production, CERN/SPSC 83-51 (1983).
[51] Design Report: An experiment at D0 to study antiproton-proton collisions at 2 TeV, December 1983.
[52] G. Arnison et al., Phys. Lett. 139B:115 (1984).
P. Bagnaia et al., Z. Phys. C. 24:1 (1984).
[53] W.J. Willis and K. Winter, *in* Physics with very high energy e^+e^- colliding beams, CERN 76-18 (1976).
[54] B.L. Beron et al., Proc. 5th Int. Conf. on Instrumentation for High-Energy Physics, Frascati, 1973. Laboratori Nazionali del CNEN, Frascati (1973), p. 362.
[55] Y. Chan et al., IEEE Trans. Nucl. Sci. NS-25:333 (1978).
[56] R. Batley et al., Performance of NaI array with photodiode readout at the CERN ISR, to be submitted to Nucl. Instrum. Methods
[57] M. Miyajima et al., Number of photo-electrons from photomultiplier cathode coupled with NaI (Tl) scintillator, KEK (Japan) 83-36 (1983).

[58] G.J. Bobbink et al., Nucl. Instrum. Methods 227:470 (1985).
[59] G. Blanar et al., Nucl. Instrum. Methods 203:213 (1982).
E. Lorenz, Nucl. Instrum. Methods 225:500 (1984).
[60] J. Ahme et al., Nucl. Instrum. Methods 221:543 (1984).
[61] J.A. Bakken et al., Nucl. Instrum. Methods 228:294 (1985).
[62] C. Laviron and P. Lecoq, Radiation damage of bismuth germanate crystals, CERN-EF/84-5 (1984).
[63] Ch. Bieler et al., Nucl. Instrum. Methods 234:435 (1985).
[64] M. Kobayashi et al., Proc. Int. Symp. on Nuclear Radiation Detectors, INS Tokyo, (1981). Inst. for Nuclear Study, Tokyo (1981), p. 465.
[65] D.E. Wagoner et al., A measurement of the energy resolution and related properties of an SCG1-C scintillation glass shower counter array for 1-25 GeV positrons, to be published in Nucl. Instrum. Methods (1985).
[66] B. Powell et al., Nucl. Instrum. Methods 198:217 (1982).
[67] W. Bartel et al., Phys. Lett. 88B:171 (1979).
[68] P.D. Grannis et al., Nucl. Instrum. Methods 188:239 (1981).
[69] K. Ogawa et al., A test of dense lead glass counters, to be published in Nucl. Instrum. Methods.
[70] R.M. Brown et al., An electromagnetic calorimeter for use in a strong magnetic field at LEP based on CEREN 25 lead glass and vacuum photo-triodes, presented at the IEEE Meeting on Nuclear Science, Orlando, Fla., 1984.
[71] C.A. Heusch, The use of Cherenkov techniques for total absorption measurements, preprint CERN-EP/84-98 (1984): invited talk given at the Seminar on Cherenkov Detectors and their Application in Science and Technology, Moscow, 1984.
[72] H. Grassmann, Untersuchung der Energieauflösung eines CsI(Tl) Testkalorimeters für Elektronen zwischen 1 GeV und 20 GeV, Universität Erlangen (1984).
H. Grassmann et al., Nucl. Instrum. Methods 228:323 (1985).
[73] M. Laval et al., Nucl. Instrum. Methods 208:169 (1983).
[74] D.F. Anderson et al., Nucl. Instrum. Methods 228:33 (1985)
[75] A. Kusumegi et al., Nucl. Instrum. Methods 185:83 (1981).
[76] H.H. Chen et al., Nucl. Instrum. Methods 150:579 (1984).
[77] E. Gatti et al., Considerations for the design of a time projection liquid argon ionization chamber, BNL 23988 (1978).
[78] K. L. Giboni, Nucl. Instrum. Methods 225:579 (1984).
[79] C. Cerri et al., Nucl. Instrum. Methods 227:227 (1984).
[80] J. Engler et al., Phys. Lett. 29B: 321 (1969).
[81] W.A. Shurcliff, J. Opt. Soc. Am. 41:209 (1951).
[82] R.C. Garwin, Rev. Sci. Instrum. 31:1010 (1960).
[83] G. Keil, Nucl. Instrum. Methods 89:111 (1970).
[84] W.B. Atwood et al., SLAC-TN-76-7 (1976).
[85] A. Barish et al., IEEE Trans. Nucl. Sci. NS-25:532 (1978).
[86] W. Selove et al., Nucl. Instrum. Methods 161:233 (1979).
[87] V. Eckardt et al., Nucl. Instrum. Methods 155:353 (1978).
[88] O. Botner et al., IEEE Trans. Nucl. Sci. NS-28:510 (1981).
[89] W. Hofmann et al., Nucl. Instrum. Methods 195:475 (1982).
[90] W. Kienzle, Scintillator development at CERN, CERN-NP Int. Report 75-12 (1975).
[91] W. Viehmann and R.L. Frost, Nucl. Instrum. Methods 167:405 (1979).
[92] J. Fent et al., Nucl. Instrum. Methods 225:509 (1984).

[93] H. Spitzer, Contribution to the Discussion Meeting on HERA Experiments, Genoa (1984);
J. Ahme et al., Novel readout schemes for scintillator sandwich shower counters, to be published.
[94] H.A. Gordon et al., Phys. Scripta 23:564 (1981).
[95] UA1 Collaboration, Technical report on the design of a new combined electromagnetic/hadronic calorimeter for UA1, CERN/SPSC/84–72 (1984).
[96] W. Kononnenko et al., Nucl. Instrum. Methods 214:237 (1983).
[97] L. Bachman et al., Nucl. Instrum. Methods 206:85 (1983).
[98] J. Borenstein et al., Phys. Scripta 23:549 (1981).
[99] H. Blumenfeld et al., Nucl. Instrum. Methods 225:518 (1984).
H. Burmeister et al., Nucl. Instrum. Methods 225:530 (1984).
[100] H. Schönbacher and W. Witzeling, Nucl. Instrum. Methods 165:517 (1979).
Y. Sirois and R. Wigmans, Radiation damage in plastic scintillators, submitted to Nucl. Instrum. Methods.
[101] G. Marini et al., Radiation damage of organic scintillation materials, CERN 'Yellow' Report, in preparation (1985).
[102] Usually, 'accelerated' tests are performed with levels of irradiation 10 to 10^6 times higher than those encountered in an experiment. Because radiation damage is frequently a function of both dose rate and integral dose, such tests are likely to indicate a higher dose tolerance than in the actual lower dose-rate experimental environment. R. Wigmans, private communication and Ref. [100].
[103] R.J. Madaras et al., Nucl. Instrum. Methods 160:263 (1979).
A.E. Baumbaugh et al., Nucl. Instrum. Methods 197:297 (1982).
A.M. Breakstone et al., Nucl. Instrum. Methods 211:73 (1982).
[104] Design report for the Fermilab Collider Detector Facility (CDF), FNAL (1981).
[105] V. Brisson et al., Phys. Scripta 23:688 (1981).
[106] W.J. Willis and V. Radeka, Nucl. Instrum. Methods 120:221 (1974).
[107] L.W. Alvarez, LRL Physics Note 672 (1968) unpublished.
[108] S.E. Derenzo et al., Nucl. Instrum. Methods 122:319 (1974).
[109] K. Masuda et al., Nucl. Instrum. Methods 188:629 (1981).
[110] T. Doke et al., Nucl. Instrum. Methods 134:353 (1976).
T. Doke, Portugal Phys. 12,1:9 (1981).
[111] G.R. Gruhn, private communication (1973).
[112] M. Conversi, Nature 241:160 (1973);
M. Conversi and L. Frederici, Nucl. Instrum. Methods 151:193 (1978).
[113] G.S. Abrams et al., IEEE Trans. Nucl. Sci. NS-27:59 (1980).
[114] V. Kadansky et al., Phys. Scripta 23:680 (1981).
[115] H.J. Behrend et al., Phys. Scripta 23:610 (1981).
[116] C. Nelson et al., Nucl. Instrum. Methods 216:381 (1983).
[117] J.A. Appel, Summary Session of the Gas Sampling Calorimeter Workshop, Fermilab FN-380 (1982);
J. Engler, Nucl. Instrum. Methods 217:9 (1983).
[118] M. Jonker et al., Nucl. Instrum. Methods 215:361 (1983).
[119] G. Battistoni et al., Nucl. Instrum. Methods 202:459 (1982).
[120] SLD Design Report SLAC-273 (1984).
[121] Presentations at the Discussion Meeting on HERA Experiments, Genoa, 1984.
[122] W.F. Schmidt and A.O. Allen, J. Chem. Phys. 52:4788 (1970).
[123] J. Engler and H. Keim, Nucl. Instrum. Methods 223:47 (1984).
[124] L. Onsager, Phys. Rev. 54:554 (1938).

[125] R.C. Munoz et al., Ionization of tetramethylsilane by alpha particles, Brookhaven Nat. Lab. C-2911 (1984), submitted to Chemical Physics Letters.
[126] G.G. Harigel, Nucl. Instrum. Methods 225: 641 (1984).
[127] P.G. Rancoita and A. Seidman, Nucl. Instrum. Methods 226:369 (1984). G. Barbiellini et al., Nucl. Instrum. Methods 235:55 (1985).
[128] E. Gatti and V. Radeka, IEEE Trans. Nucl. Sci. NS-25:676 (1978).
[129] G. Charpak and F. Sauli, Ann. Rev. Nucl. Part. Sci. 34:285 (1984).
[130] H. Videau, Nucl. Instrum. Methods 225:481 (1984).
[131] G. Battistoni et al., Nucl. Instrum. Methods 176:297 (1980).
[132] H.G. Fischer and O. Ullaland, IEEE Trans. Nucl. Sci. NS-27:38 (1980); M. Berggren et al., Nucl. Instrum. Methods 225:477 (1984).
[133] E. Iarocci, Nucl. Instrum. Methods 217:30 (1983).
[134] P. Campana, Nucl. Instrum. Methods 225:505 (1984).
[135] H. Aihara et al., Nucl. Instrum. Methods 217:259 (1983).
[136] B. Pope, Proc. DPF Workshop, Berkeley (1983), LBL-15973, p. 49.
[137] O. Botner and C.W. Fabjan, Measurements with the AFS calorimeter, unpublished note (1982).
[138] R. Diebold and R. Wagner, Physics at 10^{34} cm^{-2} s^{-1}, ANL-HEP-CP-84-87 and Proc. of the 1984 Summer Study of the Design and Utilization of the Superconducting Super Collider, Snowmass, Colo. (1984).
[139] P. Curie and A. Laborde, C.R. Acad. Sci. 136:673 (1903).
[140] S. Simon, Nature 135:763 (1935).
[141] T.O. Niinikoski and F. Udo, Cryogenic detection of neutrinos, CERN/NP Internal Report 74-6 (1974).
E. Fiorini and T. Niinikoski, Nucl. Instrum. Methods 224:83 (1984).
[142] B. Cabrera et al., Bolometric detection of neutrinos, Harvard preprint HUTP-84/A077 (1984).
[143] N. Coron et al., A composite bolometer as a charged-particle spectrometer, preprint CERN-EP/85-15 (1985).
[144] A.V. Vishnevskii et al., Moscow preprint ITEP-53 (1979).
[145] R. Bouclier et al., CERN-EP Internal Report 80-07 (1980).
[146] W.J. Willis, private communication.
[147] D.H. Perkins, Ann. Rev. Nucl. Part. Sci. 34:1 (1984).
[148] See, for example, Proc. 1980 International DUMAND Symposium, ed. V.J. Stenger. Honolulu, Hawaii (1981).
[149] R. Cady et al., Proc. 1982 DPF Summer Study on Elementary Particle Physics and Future Facilities, eds. R. Donaldson, R. Gustavson and F. Paige, p. 630.
R.M. Baltrusaitas et al., Phys. Rev. Letters 52:380 (1984).
[150] UA2 Collaboration, Proposal to improve the performance of the UA2 detector, CERN/SPSC 84-30 (1984).
[151] W.J. Willis, BNL 17522:207 (1972).
[152] See for example, Proc. DPF Workshop, Berkeley (1983), LBL-15973.
[153] E.D. Bloom and C.W. Peck, Ann. Rev. Nucl. Part. Sci. 33:143 (1983).
[154] Physics with very high energy e^+e^- colliding beams, CERN 76-18 (1976).
[155] E. Picasso, General Meeting on LEP, Villars-sur-Ollon, 1981, ed. M. Bourquin. ECFA 81/54, CERN, Geneva (1981), p. 32.

[156] The technical proposals for the four LEP experiments have the following LEP Committee numbers:
ALEPH, CERN/LEPC 83-2(1983);
DELPHI, CERN/LEPC/83-3 (1983);
OPAL CERN/LEPC/83-4 (1983);
L3, CERN/LEPC/83-5 (1983).
[157] W.K.H. Panofsky, Proc. Int. Symp. on Lepton and Photon Interactions at High Energies, Bonn, 1981, ed. W. Pfeil, Phys. Inst., Bonn (1981), p. 957.
[158] S.L.Wu, Phys. Reports 107:61 (1984).
[159] C. Rubbia, Physics results of the UA1 Collaboration at the CERN proton-antiproton Collider preprint CERN-EP/84-135 (1984): invited talk given at the Int. Conf. on Neutrino Physics and Astrophysics, Nordkirchen near Dortmund,1984.
[160] Experimentation at HERA, Proceedings of a Workshop jointly organized by DESY, ECFA, and NIKHEF, Amsterdam (1983).
[161] W. Selove, CERN/NP Internal Report 72-25 (1972).
[162] S. Almehed et al., CERN/ISRC/76-36 (1976).
[163] M.A. Dris, Nucl. Instrum. Methods 161:311 (1979).
[164] M. Block, UA1 Collaboration (CERN), unpublished note UA1-6, (1977).
[165] L. Rosselet, Proc. Topical Conf. on the Applications of Microprocessors to High-Energy Physics Experiments, Geneva, 1981, CERN 81-07 (1981), p. 316.
[166] R.L. Ford and W.P. Nelson, Stanford preprint SLAC-210 EGS, Version IV.
[167] T. Kondo et al., Talk given at the 1984 Summer Study on the Design and Utilization of the Superconducting Super-Collider, Snowmass, Colo., 1984.
DELPHI Progress Report, CERN/LEPC 84-16 (1984).
[168] A. Grant, Nucl. Instrum. Methods 131:167 (1975).
[169] H. Fesefeldt, Proc. Workshop on Shower Simulation for LEP Experiments, eds. A. Grant et al. CERN report in preparation.
[170] Proc. Workshop on Shower Simulation for LEP Experiments, eds. A. Grant et al. CERN report in preparation.